

Generation and distribution of overpressure in ultra-deep carbonate reservoirs controlled by intra-cratonic strike-slip faults: The Ordovician of Shuntuoguole area in the Tarim Basin

Shuai Zeng^{a,b}, Nansheng Qiu^{a,b,*}, Huilli Li^c, Jian Gao^c, Kangjie Long^{a,b}, Jingkun Jia^a, Xiuxiang Zhu^d

^a National Key Laboratory of Petroleum Resources and Engineering, China University of Petroleum, Beijing, 102249, China

^b College of Geosciences, China University of Petroleum, Beijing, 102249, China

^c Sinopec Petroleum Exploration and Production Research Institute, Beijing, 100083, China

^d Sinopec Northwest Oilfield Company, Urumqi, Xinjiang, 830011, China

ARTICLE INFO

Keywords:

Overpressure
Ultra-deep carbonate reservoir
Strike-slip fault
Fluid inclusion
Basin modelling
Tarim Basin

ABSTRACT

The strike-slip fault-controlled ultra-deep fractured-vuggy carbonate reservoir is an increasingly important exploration target. However, the high heterogeneity of fault-controlled reservoirs and the ineffective methods available for pressure prediction make it difficult to assess the risk of potential overpressure in ultra-deep carbonate reservoirs. Abnormal overpressure is common in the ultra-deep strike-slip fault-controlled carbonate reservoirs in the Shunbei Oilfield of the Tarim Basin. According to measured pressures, petroleum accumulation history, and fault framework, this study investigates the generation mechanisms of overpressure in fault-controlled carbonates and reconstructs the pressure evolution of reservoirs. Finally, the effect of strike-slip faults on current overpressure distribution is discussed. Measured pore pressure data from 90 wells showed that all reservoirs present in the major fault zones are normally pressured, and the reservoirs present far away from the major faults commonly develop overpressures. The distribution patterns of overpressure in the Middle-Lower Ordovician reservoirs coincide with areas with fault reactivation during the Himalayan Period. The results of the comprehensive analysis of petroleum accumulation history, fault activity, and well production suggested that dry gas generation is a primary cause of overpressure in the Middle-Lower Ordovician reservoirs. The relatively low temperature in the reservoir, in addition to the highly compartmentalized nature of overpressure, indicated that these overpressured gas migrate vertically into the Ordovician formation from deep strata along strike-slip faults. The pressure evolution restored by basin modelling and fluid inclusion showed that distinct differences in overpressure magnitude in the different reservoirs were formed at the stage of gas charging but not at the early stages of oil accumulation. The difference in physical properties of the two types of fault-controlled reservoirs resulted in different pressure distributions and oil-bearing levels in the ultra-deep carbonate reservoirs at present. The strike-slip fault zones are the primary pathways by which overpressured fluids migrate from the deeper Cambrian formation into the Ordovician reservoirs and act as barriers to separate the pressure systems in the ultra-deep carbonate reservoirs. These findings are expected to help mitigate the drilling risks with overpressure in deep strike-slip fault-controlled carbonate reservoirs.

1. Introduction

Ultra-deep high-quality carbonate reservoirs have become increasingly important targets for petroleum exploration in many petroliferous basins. However, one of the most significant challenges in developing these reservoirs is assessing the risk of potential abnormal pressure

(particularly overpressure) before drilling. Seismic velocity/porosity-vertical effective stress relationships are used to predict pore pressure in shales, and anomaly porosity that deviates from the regional normal compaction trend has been considered a direct indicator to detect abnormality in pore pressure (Bowers, 1995; Eaton, 1972; Fillippone, 1979; Swarbrick, 2001; Tingay et al., 2009; Zhang, 2011). However,

* Corresponding author. National Key Laboratory of Petroleum Resources and Engineering, China University of Petroleum (Beijing), Beijing, 102249, China.

E-mail address: qiunsh@cup.edu.cn (N. Qiu).

<https://doi.org/10.1016/j.marpetgeo.2023.106515>

Received 25 April 2023; Received in revised form 22 September 2023; Accepted 23 September 2023

Available online 27 September 2023

0264-8172/© 2023 Elsevier Ltd. All rights reserved.

during the deep burial process in most carbonates, chemically-driven diagenetic processes (chemical compaction), rather than mechanical compaction, are the principal reason for porosity reduction (Bathurst, 1972; Croize et al., 2013; Mallon and Swarbrick, 2008; Weller, 1959). Diagenesis, which includes dissolution and cementation, plays an important role in the formation and destruction of pores in deep carbonates. Secondary pores, fractures, and caverns created by the fracturing and dissolution of various fluids are usually predominant in the reservoir space in deep carbonates (Bathurst, 1972; Mazzullo and Harris, 1991; Zhu et al., 2015). Variability in carbonate porosity caused by chemically-driven diagenesis leads to inherently unpredictable velocity/porosity–depth relationships (Green et al., 2016). Therefore, considering carbonates as shales is inaccurate for pore pressure prediction in deep carbonates (Lubanzadio et al., 2002). Another problem leading to inaccurate pore pressure prediction outcomes in carbonates is that the internal physical properties of carbonate usually vary over a short distance owing to complex diagenetic processes (Bathurst, 1986; Green et al., 2016). Velocity/porosity–depth relationships provide only a local empirical fit, and these relationships are usually non-transferable unless they have a consistent lithostratigraphic context and the same overpressure generation mechanism (Drews et al., 2018; Green et al., 2016; Mohamad et al., 2015). Moreover, the restricted seismic resolution and ambiguity of seismic interpretation increase the risk of inaccurate pore pressure prediction. Published studies have reported the critical role of faults in the formation of fluid overpressure in two aspects. First, faults act as lateral seals in overpressure compartments, thus hindering the discharge of pore fluid and causing pressure cells (Carver, 1968; Dickey et al., 1968; Karlsen and Skeie, 2006; Warner, 1998); second, vertical pressure transfer through faults can induce significant changes in the pore fluid pressure of shallower formations (Grauls and Baleix, 1994; Karthikeyan et al., 2020; Luo et al., 2003; Zhang et al., 2023). Petroleum reservoirs with overpressure compartments have been extensively discovered in extensional and compressional foreland basins, and their distribution patterns have been investigated in a detailed manner (Byerlee, 2013; Darby and Funnell, 2001; Guo et al., 2016; Karthikeyan et al., 2020; Luo et al., 2007; Madon, 2007; Rice, 1992). However, different types of basins (such as extensional, compressional, and strike-slip basins) have distinct stress states, which create inevitable differences in their pressure fields (Yassir et al., 2002).

The ultra-deep fault-controlled fractured-vuggy reservoirs in China's three largest cratonic basins (namely, Tarim, Sichuan, and Ordos basins) have large petroleum resources (Ma et al., 2022; Zheng et al., 2022). Strike-slip faults play an important role in the development of fractured-vuggy reservoirs and petroleum accumulation (Deng et al., 2022; Liu et al., 2023; Qi, 2020; Wang et al., 2022; Yu et al., 2022). However, the distribution patterns of overpressure in strike-slip fault-controlled carbonate reservoirs have received less attention (Ozkale, 2007; Peacock et al., 2017). The Shunbei Oilfield, which is the world's deepest commercially developed oil and gas field, offers plentiful petroleum resources in the Ordovician reservoirs. However, a series of overpressure compartments have been discovered in the strike-slip fault-controlled carbonate reservoirs with an average burial depth of more than 7200 m. Most published studies suggested that the Carboniferous–Devonian strata are extensively overpressured, and the Ordovician carbonates are normally pressured in the cratonic region of the Tarim Basin (Liu et al., 2013, 2019; Lu et al., 2016a; Sun, 2003; Wang and Ye, 1998). Sun (2003) performed a statistical analysis of pressure testing data from more than 200 wells and reported that the average pressure coefficient of the Ordovician carbonate reservoirs in the Tabei Uplift is 1.10. Liu et al. (2019) reported that the maximum residual pressure of Ordovician carbonate reservoirs with a burial depth of more than 5000 m in the Tazhong Uplift is only 8 MPa. The discovery of strong overpressured carbonate reservoirs in the Shuntuoguole Low Uplift is contradictory to previously reported findings of the pressure state of the Ordovician carbonate strata. Therefore, it is important to explore overpressure formation and preservation in ultra-deep

carbonate reservoirs and consider the possible effects of strike-slip faults on fluid pressure.

This study presents a comprehensive geological approach to gain a better understanding of overpressure formation and preservation in deep marine carbonate strata controlled by intra-cratonic strike-slip faults. The study combined geological factors with the characteristics of overpressured reservoirs to unravel the main reason for overpressure formation in fault-controlled reservoirs. The pressure evolution of these carbonates was reconstructed by basin modelling software and fluid inclusion PVT (pressure-volume-temperature) simulation. By linking overpressure formation with pressure evolution, the present-day pressure distribution patterns of deep carbonates were determined in light of the hydrocarbon accumulation history and fault framework. The findings of this study are expected to provide a better understanding of overpressure distribution patterns in deep burial carbonate reservoirs controlled by strike-slip faults.

2. Geological background

The Tarim Basin, located in northwest China (Fig. 1A), is the largest area for ultra-deep oil and gas resources in China, and it is estimated to have approximately 8.25 billion tons of recoverable reserves (Yang et al., 2021c). This basin is a microcontinent and has undergone long-term complex tectonic evolution, multi-stage transformation, and deformation (An et al., 2009; Wu et al., 2021; Yang et al., 2021b). The study site in this area is the Shuntuoguole Low Uplift (SLU), situated in the lower part of the structure between the two ancient uplifts of Tabei and Tazhong in the Tarim Basin. The study site is divided into four secondary tectonic spanning units from northwest to southeast: Shunbei Slope (SB), Shuntuo Low Uplift (ST), Shundong Slope (SD), and Shunnan Slope (SN) (Fig. 1B and C).

During the Early Cambrian to Middle Ordovician, the Tarim Basin was in the stage of weak extension and was inundated by seawater owing to extensive transgression (Wu et al., 2020a; Zhang et al., 2015a). The SLU area was located in the center of a large cratonic carbonated platform with thick carbonate deposits. During the Middle Ordovician, the Tarim Basin underwent north-south compression owing to the subduction of the proto-Tethys Ocean. The northeast-oriented strike-slip fault zones of the SLU area started emerging because of the stress-induced transition from extension to compression (Yang et al., 2020). During the Late Ordovician, the depositional environment of the SLU area evolved as a coastal and shallow sea (Wu et al., 2020a). The Late Ordovician successions consist of marine clastic rocks with a thickness of 500–1400 m in the SLU area, but these strata are absent in most regions of the Tazhong Uplift and Tabei Uplift. The SLU area evolved as a coastal, shallow sea and predominantly depositions of thick clastic rocks since the Silurian. When the Tarim Basin entered the stage of intense extrusion, the basin underwent extensive uplifting and erosion in the Late Silurian, which caused the absence of the top of the Upper Silurian and the Middle-Lower Devonian in the SLU area. The inherited strike-slip faults, which had intense activity, divided the study site into several blocks and appeared as high-steep vertical faults or flower-shaped structures on the section (Fig. 2). With the gradually retreating seawater, the basin's sedimentary environment has undergone a transformation from marine facies and marine-continental alternation facies to fluvial lacustrine continental facies during the Late Permian (Wu et al., 2020a). During the Mesozoic, the Tarim Basin, which is surrounded by orogenic belts, experienced frequent tectonic movement and severe erosion (Fig. 2). Since the Neogene, the Tarim Basin experienced rapid deposition owing to the remote effect of the intense collision of the Indian plate (Jia, 2004; Xu et al., 2011). The SLU area located far away from the areas affected by the strong compressive stress, which resulted in strike-slip fault activity is weak in the deep regions of the study site. (Jia et al., 2022). The Neogene and sedimentary sequences consist of terrestrial clastic rocks with a thickness of 2200–3300 m.

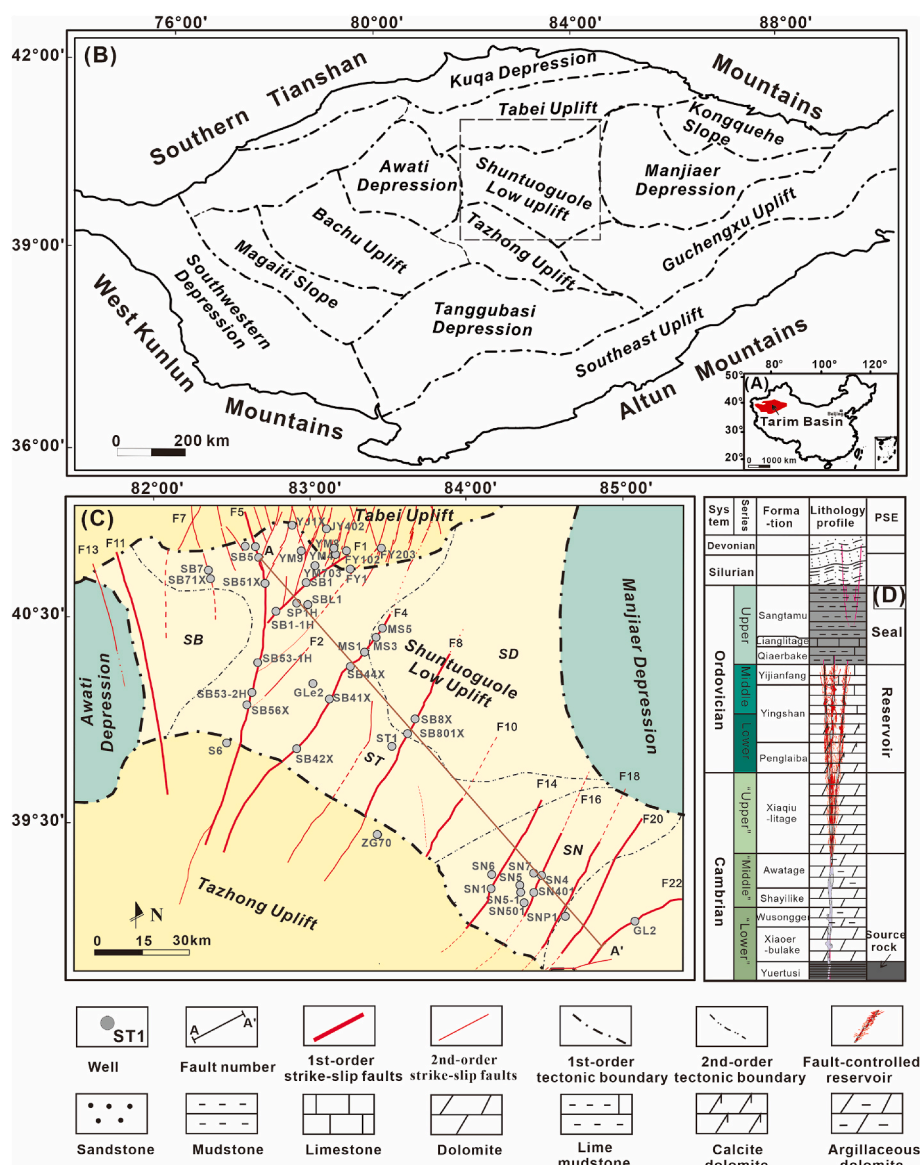


Fig. 1. (A) The geographic location of the Tarim Basin in northwestern China. (B) Location map showing the tectonic units of the Tarim Basin and location of the Shuntuoguole Low Uplift (modified after Yu et al. (2022)). (C) The division of structural units in Shuntuoguole Low Uplift and the study well locations in this paper. (D) The stratigraphic column with petroleum systems elements (modified after Ma et al. (2022)).

The strike-slip faults present in the SLU area have a relatively minor slip distance of less than 2 km and are termed as intra-craton strike-slip faults (Deng et al., 2019; Han et al., 2017). The present-day fault pattern of the SLU area and its surrounding area is generally bounded by the N45°E-oriented F1 fault zone, comprised of two distinct strike-slip fault systems in the south and north (Deng et al., 2022; Ma et al., 2012; Wu et al., 2012). The northern area is characterized by an “X”-shaped conjugate fault system formed by northwest-oriented and northeast-oriented strike-slip faults, whereas the southern area predominantly has a single row of Northeast-oriented left-slip fault systems (Fig. 1C). During the Late Himalayan, the Northeast-oriented fault belts (F1, F4, and F8) in the central part of the SLU area had weak inherited activities. In contrast, the Northeast-oriented faults in the SN area and northwest-oriented faults remained inactive after the Middle-late Hercynian and the Late Caledonian, respectively (Yun, 2021).

The Cambrian and Ordovician carbonate rocks and marine shale constitute a complete source-reservoir-cap assemblage in the Tarim Basin (Fig. 1D). The significance of Cambrian source rocks is gradually gaining attention, as many petroleum resources have been discovered in

the deep reservoirs (Zhu et al., 2022). The Lower Cambrian Yuertusi formation, widely distributed in the Tarim Basin, is a set of high-quality source rocks with a total organic carbon content between 2% and 16% (Wei et al., 2021; Zhu et al., 2016a). The Middle and Lower Ordovician (O₁₋₂) fault-controlled fractured-vuggy carbonates are the most important petroleum reservoirs in the SLU area, which comprises the reservoir-seal pairs with the overlying thick marine mudstone of the Upper Ordovician. The strike-slip faults connect the Cambrian source rocks with the Middle and Lower Ordovician reservoirs, providing permeable conduits and space for petroleum transportation and storage (Deng et al., 2022; Jiao, 2017; Qi, 2016).

3. Database and methods

The direct pressure test is the most reliable method to obtain fluid pressure in the permeable layers (Lee et al., 2022). For low or non-permeable layers (such as mudstone and salt rock), fluid pressure is calculated based on well-logging, mud density, and various response characteristics (Bowers, 1995; Eaton, 1972; Fillippone, 1979; Radwan,

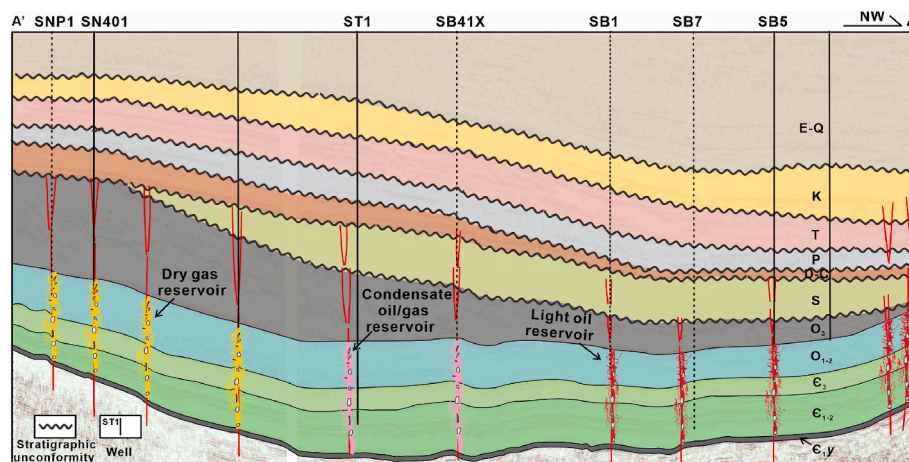


Fig. 2. Seismic section showing the stratigraphic distribution and the developments of strike-slip faults-controlled reservoirs.. (E–Q: Paleogene to Quaternary, K: Cretaceous, T: Triassic, P: Permian, D–C: Devonian to Carboniferous, S: Silurian, O₃: Upper Ordovician, O₁₋₂: Middle-Lower Ordovician, C₁: Upper Cambrian, C₁₋₂: Middle-Lower Cambrian, C_{1-2y}: Lower Cambrian Yuertusi formation.)

2022; Swarbrick and Lahann, 2016). However, in the absence of continuous pressure testing, mud weight is often used as a proxy for pore pressure, which will help understand the characteristics of pressure variation as depth increases (Webster et al., 2011). However, mud weight is not always a valid proxy for pore pressure. Therefore, in this study, we performed a careful comparison between mud equivalent pressure and drill stem test data and selected mud weights consistent with the pressure measurement data so as to provide a general guide for judging the vertical trend of the pore pressure. The study collected drill-stem test pressure data of 90 wells present in the Middle and Lower Ordovician formations in the SLU area, and complementary mud weight data of those wells. This study used the pressure coefficient (ratio of pore pressure to hydrostatic pressure at the same depth) as a measure to determine the presence and magnitude of overpressure. The pressure coefficient was categorized as follows: ≤ 1.20 indicates normal pressure, ≥ 1.20 indicates overpressure, and ≥ 1.60 indicates strong overpressure.

Fault-controlled carbonate reservoirs have storage spaces of various sizes and intricate connection variances (Deng et al., 2022; Wu et al., 2020b). The static characteristics of reservoirs with overpressure and those with normal pressure were determined by core samples and formation micro scanner image logging (FMI). Additionally, the dynamic seepage characteristics of these reservoirs were compared by build-up curves and production data.

For microscopic fluid inclusion analyses, core samples were collected from eight wells (SB5, GL2, MS5, ST1, SN1, SN4, SN501, GL2). Fluid inclusion micro thermometry analysis was performed at the National Key Laboratory of Petroleum Resources and Engineering of China University of Petroleum (Beijing). The LINKAM THMS-G600 temperature-controlled stage was used in the experiment, which has a temperature measurement range of $-196\text{ }^{\circ}\text{C}$ – $600\text{ }^{\circ}\text{C}$. The accuracy of the freezing and heating data was $\pm 0.1\text{ }^{\circ}\text{C}$ and $\pm 2\text{ }^{\circ}\text{C}$, respectively. The effectiveness of fluid inclusion homogenization temperatures was evaluated based on the fluid inclusion assemblage (FIA) concept (Goldstein and Reynolds, 1994; Liu et al., 2013). In this research, the measured homogenization temperature is considered reliable only when the difference between the temperature measurements of FIA is less than $15\text{ }^{\circ}\text{C}$ (Liu et al., 2013).

Gas-phase and gas-liquid two-phase inclusions in minerals were analyzed using Raman spectroscopy to identify the gas-phase components (Caumon et al., 2014). The Laser Raman spectroscopy was performed using the Renishaw inVia Reflex Laser Raman spectrometer. The Raman characteristic peak of methane gas in the standard sample was detected at 2917.58 cm^{-1} at room temperature. The laser source used in the experiment had a wavelength of 532 nm , and the integration time was set to 25 s with a total of 10 integration times.

Under the same temperature and pressure conditions, coeval aqueous inclusions and petroleum inclusions were trapped simultaneously (Aplin et al., 1999, 2000; Karlsen et al., 1993; Nedkvitne et al., 1993; Pironon and Bourdet, 2008). Therefore, the trapping pressure was determined mainly by combining the isochoric lines of the two systems (Aplin et al., 2000; Goldstein and Reynolds, 1994; Mullis, 1979). As for fluid composition, the hydrocarbon components were assumed to the approximate composition in oil inclusions. The assumed composition can be simulated when the gas-liquid ratio obtained by iterative calculation had to be consistent with the measured values of inclusions at room temperature. Based on the assumed fluid composition proxy, the isochoric lines of coeval brine inclusions and hydrocarbon inclusions were simulated using the equation of state (Aplin et al., 1999, 2000).

A specific method was used to determine the trapping pressure of gas inclusions, assuming that both the gas and liquid phases of the inclusions are homogeneous at the saturation pressure with the gas dissolving completely (Liu et al., 2018; Zhang et al., 2015b). This method involved six steps and was performed according to the method described by Liu et al. (2018) and Zhang et al. (2015b): (1) The initial composition and percentage components of the gas phase of inclusions were determined by the present-day composition of the gas reservoir. (2) The pressure was adjusted continuously according to the homogenization temperature of the inclusions until the “vapor” value in PVTsim equaled zero. At this point, the pressure should be the minimum trapping pressure of the assumed initial inclusions, and the total molar volume should be determined. (3) The gas–liquid ratio of the inclusions at room temperature was calculated based on the initial composition. If the calculated ratio does not match the measured value, the input component was adjusted until both values were consistent. (4) The minimum trapping pressure was calculated by inputting the equivalent component, homogenization temperature, and total volume of the inclusion. (5) The previous steps were repeated at a temperature slightly higher than the homogenization temperature for the total volume to determine another pressure value. By combining the two temperatures with the associated pressures, we established the pressure-temperature equation for the gas-bearing inclusions. (6) The trapping temperature of the brine inclusions associated with gas inclusions was used to determine the trapping pressure by establishing line equations and was projected onto the burial/thermal history to determine their trapping time and paleo depth (Karlsen et al., 1993; Matapour and Karlsen, 2017).

After accurate calibration of the Raman spectroscopic system, the Raman shift of the C–H symmetric stretching band of methane can be used to quantitative determine the internal pressure of methane-bearing inclusions under a closed system (Dubessy et al., 2001; Fabre and Couty,

1986; Gao et al., 2017; Lin et al., 2007; Lu et al., 2007a). The gas composition from the separator test by PVT testing was selected as the initial composition for simulation. The gas components were repeatedly changed to simulation until the gas-liquid ratio and internal pressure matched the measured value at room temperature, and the equivalent gas component and corresponding inclusion volume were determined. If the inclusion volume remained constant, the trapping pressure was calculated based on homogenization temperature and inclusion volume. Only in the case of mixtures of CH₄ with low concentrations (<10 mol %) of other components, this study simplified these inclusions to methane system, and used the formula developed by Lu et al. (2007b) to assess methane density in the inclusions, then calculated the trapping pressure by the thermodynamic equation established by Duan et al., 1992.

Basin models are used to quantitatively evaluate some fundamental processes of overpressure formation and their efficiency (Hantschel and Kauerauf, 2009). Because the estimation of fluid inclusion provides only single-point information at a particular time, this study used Petro-Mod2012.1 software to reconstruct fluid pressure evolution during the burial period. The distribution of strata and lithology was based on drilling wells' cutting data, and various mixing ratios were applied to different components to ensure that modelled lithologies were consistent with the lithologic components of the actual strata (Table 1). The sedimentary age and durations of each unit were determined from published literature. The erosional thickness and denudation time of tectonic erosion events were determined from the results published by Zhang et al. (2000), and the thermal boundary conditions in basin modelling were derived from Liu et al. (2020) and Qiu et al. (2012).

The Athy formula and Kozeny-Carman equation were used to quantify the porosity-depth relationship and the porosity-permeability relationship in the models, respectively (Hantschel and Kauerauf, 2009). The Easy Ro% model proposed by Sweeney and Burnham (1990) was used for reconstructing the maturity evolution of source rock, and the Burnham TII Kinetics model proposed by Burnham and Sweeney (1989) was applied to simulate hydrocarbon generation. The kerogen type, TOC (total organic carbon) content, and HI (hydrogen Index) were referred to by Zhu et al. (2016b) and Wei et al. (2021).

The pore pressure equation combined with the overpressure equation related to petroleum generation to calculate the magnitude of overpressure in this model, and these two equations were proposed by Hantschel and Kauerauf (2009). The sensitivity of pressure solution depends on the connectivity of the highly permeable facies, and the two

lithological parameters, compressibility and permeability control fluid flow and pressure formation (Hantschel and Kauerauf, 2009). These parameters are adjusted until a satisfactory match is reached between the modeled and the actual geological pressure.

4. Results

4.1. Present day pressure of the reservoir

The pressure test data revealed that abnormal overpressure had developed and was widely distributed in the Middle-Lower Ordovician carbonated reservoirs in the SLU areas. However, significant differences existed in the pressure states of three secondary structural units (Fig. 3). Particularly, the pressure coefficient in the Middle-Lower Ordovician reservoirs in the Tabei Uplift in the northern margin of the study area ranged from 1.01 to 1.47. By contrast, no overpressure reservoirs were discovered in the adjacent SB area. The ST area showed a mix of normal pressure and locally developed strong overpressure, with the pressure coefficient ranging from 0.96 to 1.79. The SN area was characterized by overall overpressure, with the pressure coefficient ranging from 1.17 to 1.65. Regarding lateral distribution, the pressure coefficient tended to increase from the northern to the southern tectonic unit gradually. However, the reservoir with the maximum pressure coefficient was observed near the Northeast-oriented faults in the ST area. Strike-slip faults separated the basin into many isolated pressure systems (Fig. 3). The reservoirs with normal pressure were mainly distributed in bands following the direction of major strike-slip faults, while reservoirs with overpressure were distributed between the fault zones or on the secondary inner faults (Figs. 3 and 4). Additionally, the reservoirs located in different sections of the same strike-slip fault zones were segmented, but they did not show any discernible difference in the pressure state and all were in the normal pressure state (Figs. 3 and 4).

The significant variation in drilling mud density observed in the Middle-Lower Ordovician reservoirs indicated the presence of at least two distinct pressure structures in the study area. For wells far from the major fault zones, the equivalent fluid pressure lines calculated based on mud density demonstrated gradual deviation from the hydrostatic pressure curve in the Carboniferous strata and exhibited significant deviation from the hydrostatic pressure curve at the top of the Ordovician. The different variation trends in equivalent fluid pressure indicated the presence of at least two vertical overpressure systems: the C–O₃ weak overpressure system and the O₂–S overpressure system (Fig. 5A

Table 1
Modeled stratigraphy and input parameters for modelling wells.

| Strata/event | Begin age (Ma) | Litho mixture ration (%) | Present or erosion thickness (m) | | | | |
|--------------------|----------------|---------------------------|----------------------------------|-------|------|-------|-------|
| | | | SB5 | GL2 | MS5 | SN5 | SN4 |
| N + Q | 23 | 30ss, 40sil, 30sh | 3066 | 2242 | 2200 | 1003 | 1005 |
| E | 65 | 40sil, 60sh | 120 | 162 | 166 | 730 | 723 |
| EROSION 6 | 80 | | –190 | –200 | –200 | –120 | –120 |
| K | 137 | 60ss, 40sh | 832 | 683 | 918 | 376 | 407 |
| EROSION 5 | 210 | | –400 | –400 | –400 | –350 | –350 |
| T | 251 | 50ss, 30sil, 20sh | 756 | 793 | 578 | 605.5 | 538.5 |
| EROSION 4 | 258 | | –40 | –40 | –40 | –40 | –40 |
| P | 290 | 45dia, 25il, 30sh | 533 | 501.5 | 546 | 445 | 384 |
| EROSION 3 | 300 | | –210 | –210 | –210 | –130 | –130 |
| C | 350 | 20ss, 10sil, 50sh, 20lime | 262 | 175 | 526 | 581 | 594 |
| D | 370 | 30ss, 30sil, 40sh | 144 | 163.5 | 17 | 85 | 80 |
| EROSION 2 | 428 | | –260 | –260 | –260 | / | / |
| S | 440 | 30ss, 30sil, 40sh | 1078 | 1146 | 1066 | / | / |
| EROSION 1 | 445 | | –130 | –130 | –130 | –100 | –100 |
| O ₃ | 460 | 80sh, 20lime | 537 | 1333 | 1480 | 2591 | 2673 |
| O ₂ y | 470 | 100lime | 92.2 | 153 | 172 | 141.5 | 144 |
| O ₁₋₂ y | 480 | 100lime | 607.8 | 594 | 564 | 414.5 | 452 |
| O ₁ p | 490 | 80lime, 20dol | 390 | 328 | 350 | 432 | 459 |
| C | 521 | 100dol | 2020 | 2863 | 2863 | 1280 | 1300 |
| C ₁ y | 541 | 100sh | 30 | 20 | 20 | 20 | 20 |

ss = sandstone; sil = siltstone; sh = shale; dia = diabase; lime = limestone; dol = dolomite, the absolute value of the negative number indicates the erosional amount.

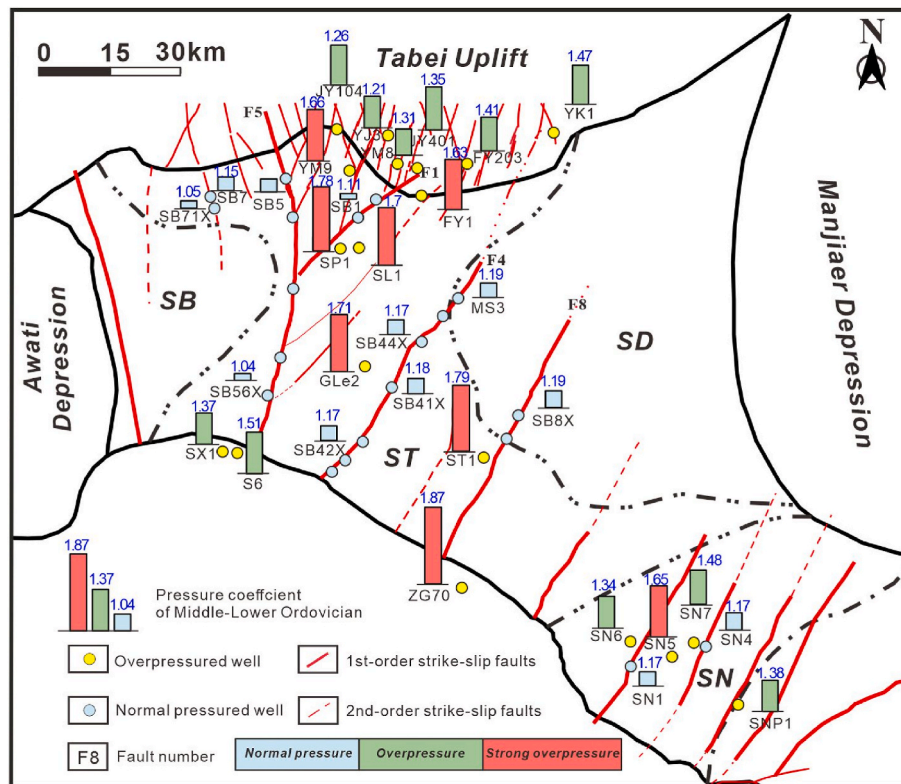


Fig. 3. Distribution of wells with abnormal pressured and overpressured Middle-Lower Ordovician reservoir and strike-slip faults in the Shuntuoguole area. (Strong overpressure: Pressure coefficient >1.6 , Overpressure: Pressure coefficient >1.2 , Normal overpressure: Pressure coefficient <1.2).

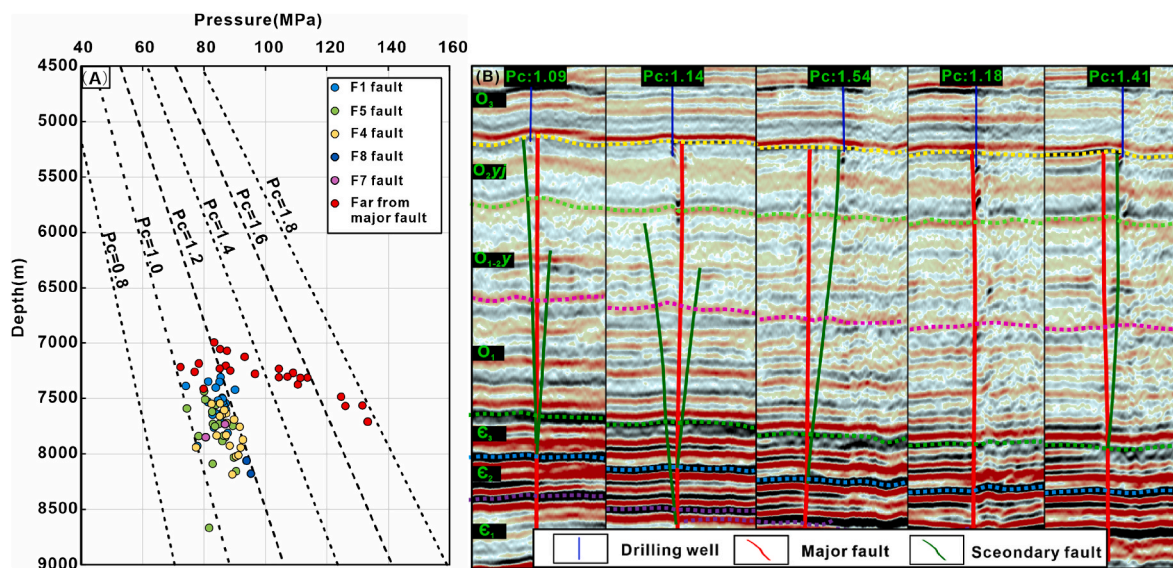


Fig. 4. The distribution of present pressure in the Middle-Lower Ordovician reservoir from different fault zones. Reservoirs near the major fault appear to be normally pressured (Pressure coefficient (Pc) <1.20), and reservoirs far away from the major fault seem to be overpressured (Pc >1.20).

and B). However, when drilling into the core of the fault zone, the fluid pressure significantly decreased, indicating that abnormal pressure has not developed in the Middle-Lower Ordovician reservoirs in this area at present (Fig. 5C).

4.2. Overpressure reservoir characteristics

A comprehensive analysis of the dynamic and static reservoir characteristics was performed in strike-slip fault-controlled carbonate

reservoirs with overpressure and those with normal pressure in the SLU area. The formation micro-scanner image (FMI) logging data showed that the carbonated reservoirs with overpressure were characterized by fractures (Fig. 6A). During drilling encounters in the reservoir with overpressure, slight or no leakage of drilling mud occurred, and the pressure build-up curve was characterized by bilinear flow. The exploited fractured reservoirs produced a large volume of water, and the pressure dropped rapidly (Fig. 6C; Table 2). These dynamic and static characteristics indicated that reservoirs with overpressure had a

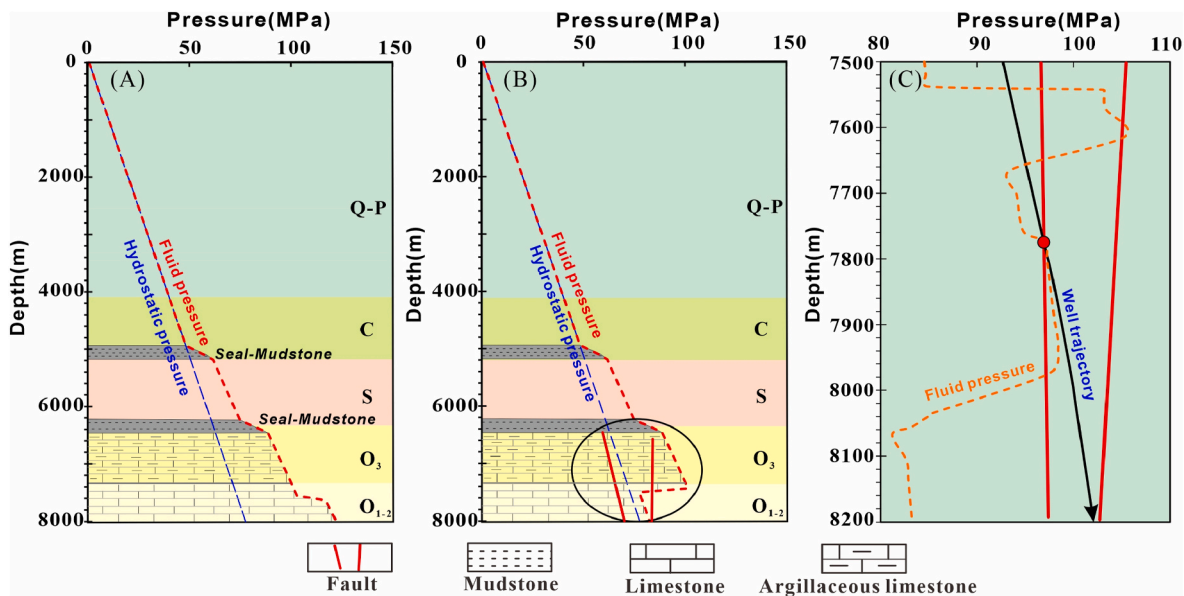


Fig. 5. Validated equivalent fluid pressure calculated by mud density suggested there are two kinds of pressure structures in the Shuntuoguole area. The circle part of (B) is magnified and shown in (C) to display that fluid pressure decreases significantly in reservoirs when drilling into the major fault zone.

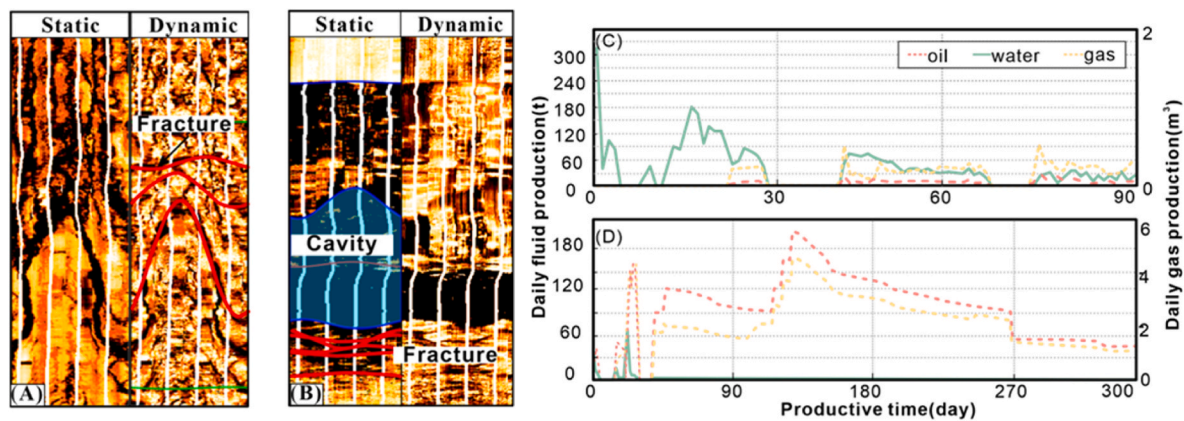
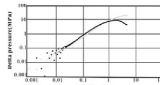
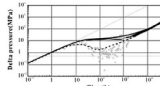


Fig. 6. Formation micro-scanner image (FMI) of overpressure reservoir and normal pressure reservoirs and their daily production. The Middle-Lower Ordovician reservoir with a pressure coefficient of 1.70 is characteristic of fractures, and high water-yield (A, C). The reservoir with a pressure coefficient of 1.15 is characterized by fractures and cavities and high-yield petroleum (B, D). These two wells are present in the major fault and around this fault.

Table 2
Dynamic and static characteristics of overpressured carbonate reservoirs.

| Reservoir type | Pressure coefficient | Location | Pressure build curve | Drilling into the cave and mud loss | Formation testing |
|--------------------------|----------------------|------------------------------|---|--|---|
| Fractured reservoir | 1.70 | Secondary inner fault |  | Slight or no leakage | High yield water and yield condensate gas, oil pressure drops quickly |
| Fracture-vuggy reservoir | 1.15 | Major strike-slip fault zone |  | Drilling into caves and lots of mud losses | High-yield condensate oil |

relatively small reservoir scale and lacked connectivity with the outside reservoirs. By contrast, normal-pressured reservoirs developed many fractures and cavities (Fig. 6B). Drilling into cavities and mud losses often appeared in reservoirs with normal pressure in the major fault zones. The pressure build-up curve showed adequate capacity for reservoir and percolation (Table 2). Normal pressured fractured-vuggy

reservoirs in the exploitation had produced a large volume of petroleum (Fig. 6B). The comparison of the dynamic and static characterizations of reservoirs under different pressure states suggest that the connectivity of the strike-slip fault with the outside and the reservoir scale may be critical to the formation of abnormal pressure.

4.3. Petroleum accumulation history

A large number of fluid inclusions are distributed within the fracture-filling calcite veins, appearing as isolated groups or trails. They occurred as single-phase inclusions (only oil, water, or gas), liquid-dominated bi-phase inclusions (water–gas, oil–gas), and tri-phase fluid inclusions containing solid bitumen (oil, gas, and solid bitumen). Comprehensive analysis of microscopic petrography and cathodoluminescence characteristics suggested that there are at least three stages of calcite veins in Middle-Lower Ordovician formations (Fig. 7). These calcite veins had obvious cutting characteristics and the occurrence of secondary inclusions with blue fluorescence in the heal fractures. In situ U–Pb dating of calcite veins suggested that these calcites were respectively formed at 474–444 Ma, 441–403 Ma, and 374–326 Ma, as well as 295.9–232 Ma, which were consistent with the periods of fault activity analyzed by seismic profile (Li et al., 2023). Calcite-filling U–Pb dating constrains the onset of late oil charge to the Late Permian.

These oil-bearing inclusions appeared colorless and transparent or

brown under transmitted light and emitted green-yellow and blue-white fluorescence under ultraviolet fluorescence (Fig. 8A–G). Inclusion oils with different physical chemistry properties usually exhibit different fluorescence colors under ultraviolet fluorescence, which is a significant indicator of distinguishing different generations of inclusions (Goldstein and Reynolds, 1994; Ryder, 2005). By reducing the artificial error in the determination of fluorescence color by the naked eye, micro-fluorescence spectroscopy can be used to evaluate the maturity of oil inclusions accurately (Liu et al., 2009; McLimans, 1987; Stasiuk and Snowdon, 1997). The Microfluorescence spectra of different petroleum inclusions reveal apparent differences in thermal maturity of the two types of oil inclusions (Fig. 9), and suggest that at least two stages of oil have filled into the Ordovician reservoirs in the study area. Liquid-dominated bi-phase inclusions (water and gas) and single-vapor inclusions were detected in SN5 samples, and oil-bearing inclusions with fluorescence were rarely observed (Fig. 8H and I).

Homogenization temperatures reflect the trapping temperature only when the water or oil in the fluid inclusions is saturated with respect to

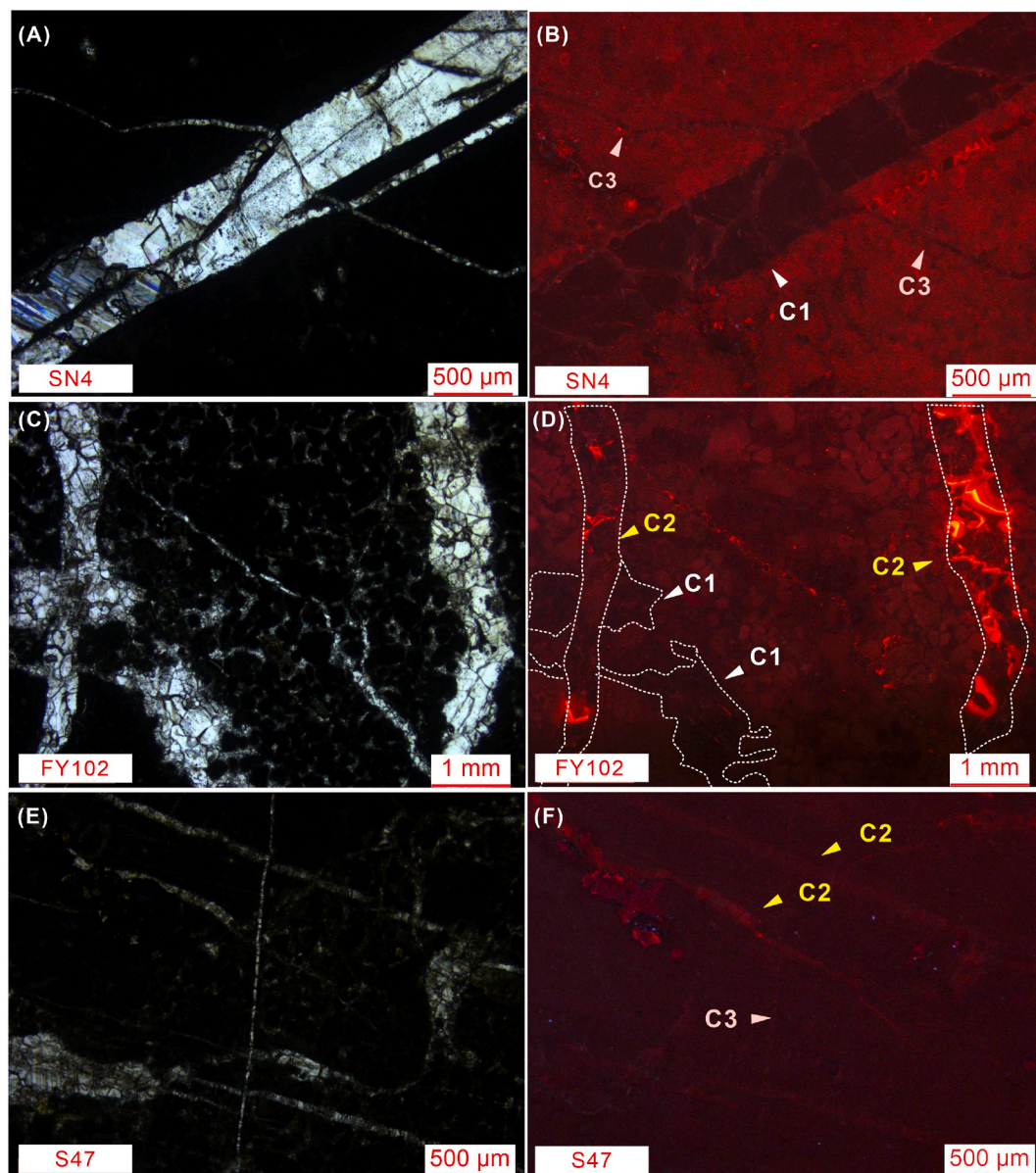


Fig. 7. Plane-polarized light (PPL) and cathodoluminescence photomicrographs showed that there are three stages of calcite veins with cutting characteristics. C1 exhibited dark red cathodoluminescence characteristics under cathode rays. C2 exhibited bright red cathodoluminescence under a cathode ray. C3 had no luminescence under a cathode ray.

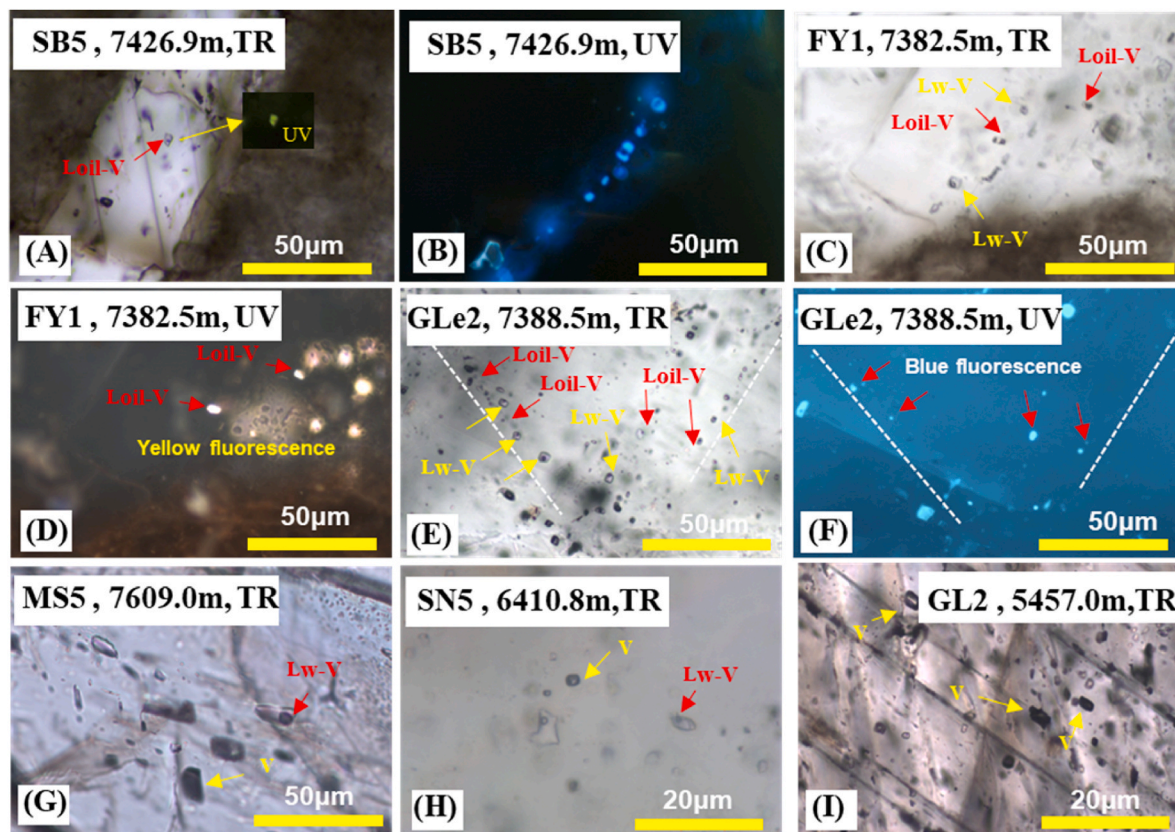


Fig. 8. Photomicrographs of fluid inclusions in the fractured-filling calcite in the Middle-Lower Ordovician reservoirs. (A) Yellow fluorescence hydrocarbon inclusions under UV light. (B) Trail distribution hydrocarbon inclusion with blue fluorescence under UV light. (C) Coeval aqueous inclusions associated with oil inclusions. (D) Yellow fluorescence oil inclusions under UV light. (E) Oil inclusions and coeval aqueous inclusions in healed micro-fracture. (F) Group distribution oil inclusions with light blue fluorescence under UV light. (G) Vapor-single and liquid-vapor biphasic hydrocarbon inclusions co-exist in calcite. (H) Group distribution gas inclusions with vapor-single phase and liquid-vapor biphasic. (I) Group distribution vapor single inclusions. Loil = Liquid oil, V=Vapor, Lw = Liquid water.

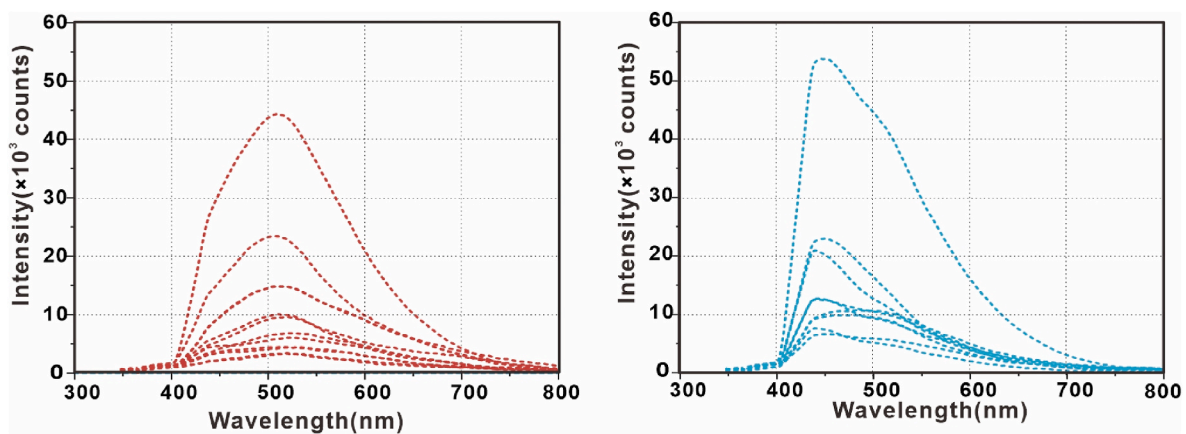


Fig. 9. The fluorescence spectrum shows the maturity of different oil inclusion in the SLU area.

gas (Goldstein and Reynolds, 1994; Karlsen et al., 1993; Nedkvitne et al., 1993; Roedder, 1972). In a system with co-existing oil and aqueous inclusions, the gas content in aqueous inclusions will likely be very close to or reach saturation, but petroleum inclusions are likely to be under-saturated (Bhullar et al., 1999; Matapour and Karlsen, 2017; Matapour et al., 2019). Considering the potential risk of fluid inclusion re-equilibration in the calcite (Bourdet et al., 2008; Larson et al., 1973; Prezbindowski and Larese, 1987), the minimum homogenization temperatures of the aqueous inclusions coeval with petroleum inclusions were applied to reflect the minimum trapping temperature for the oil

inclusions. By projecting the homogenization temperature of fluid inclusions onto the basin burial history curve, the timing of the petroleum charge can be determined (Karlsen et al., 1993). The homogenization temperature of aqueous inclusions associated with yellow-fluorescent oil inclusions ranged from 70 °C to 90 °C and 85 °C to 110 °C in wells SB5 and GLe2, respectively (Fig. 10), corresponding to the oil accumulation during the Late Caledonian (Fig. 11). The homogenization temperature of aqueous inclusions associated with blue-white fluorescent oil inclusions ranged from 100 °C to 125 °C and 120 °C–135 °C in wells SB5 and GLe2, respectively (Fig. 10), corresponding to the oil

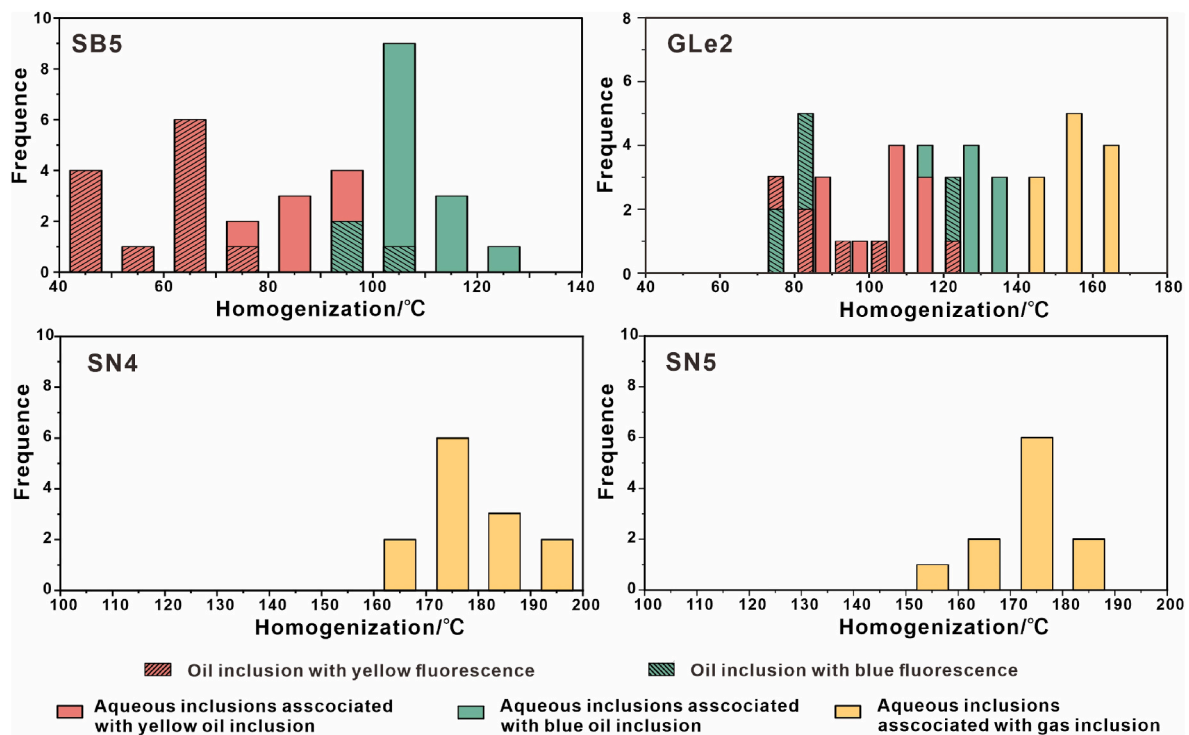


Fig. 10. Homogenization temperature histograms of petroleum and associated aqueous inclusions, showing the temperature of petroleum filling and entrapment in different stages.

accumulation during the Late Hercynian (Fig. 11). The homogenization temperature of gas-water bi-phase inclusions associated methane inclusions in well GLe2 ranged from 145 °C to 165 °C, which indicated that gas formation occurred mainly during the Himalayan Period (Figs. 10 and 11).

4.4. Paleo-pressure recovered from fluid inclusions

Fluid inclusion is an effective method for determining the pressure of the diagenetic fluid, which is based on the hypothesis that the initial physical and chemical properties of the fluids can be recorded in inclusions under well preservation (Aplin et al., 1999; Goldstein and Reynolds, 1994; Pironon and Bourdet, 2008). However, the fluid inclusions in carbonate minerals are prone to leakage of initially entrapped fluid and filling with other diagenetic fluid by thermal or barometric stress, which led to changes in the volume and composition of fluid inclusions (Bourdet et al., 2008; Goldstein and Reynolds, 1994). Fluid inclusions with relatively low Th and gas volume percentages in a fluid inclusion assemblage were selected to recover paleo-pressure in this study, because they were likely to preserve the initial composition of the fluid. The hydrocarbon composition from Middle-Lower Ordovician in well SB5 was selected to be the initial composition for simulation (Table 3), because of low maturity and less gas charge. The gas composition from the separator test by PVT testing was selected as the initial composition for the simulation of methane-bearing inclusions (Table 3).

The pressure state of the reservoir during key accumulation periods was evaluated by the restored trapped pressure of hydrocarbon inclusions formed in different geological periods using fluid inclusion PVT simulation. Samples from the Ordovician reservoirs present in the major fault zones (SB5, MS5, SN1, SN4, and GL2), and samples from the reservoirs present far away from major fault zones (GLe2, ST1, SN501, and SN5) were used to restore the paleo-pressure of the Middle-Lower Ordovician reservoirs. The method proposed in Section 3 was applied to calculate the trapping pressure of petroleum inclusions. Tables 4–6 present the results of paleo-pressure restored by fluid inclusions. The

paleo-pressure coefficient of the Middle-Lower Ordovician reservoir in well SB5 ranged from 1.00 to 1.01, and the pressure state in the two oil accumulations is characterized by normal pressure. Similarly, in well FY1, the paleo-pressure state of the reservoir developed normal pressure during the late Caledonian and Hercynian Periods, with pressure coefficients of 1.03 and 1.12, respectively.

Gas-bearing inclusions were observed in the Middle-Lower Ordovician reservoir located in the SLU area. The gas components in these inclusions were analyzed at room temperature using a Laser Raman spectrometer, and the Raman shifts indicated that methane was the predominant component in the vapor phase (Fig. 12). To reduce uncertainty, three methods were used to calculate the pressure of the gas-bearing inclusions. The results showed that the pressure coefficients of the Middle-Lower Ordovician reservoir far from major faults during the Himalayan Period were generally above 1.60, and higher than those in samples collected from areas near major faults (Tables 5 and 6). The paleo-pressure, as restored by the gas-bearing inclusions, supports the possibility that gas formation led to strong overpressure in the carbonate rocks present in the research area.

5. Discussion

5.1. Effect of strike-slip faults on overpressure generation

The generation of abnormal overpressure in the sedimentary basins can be classified into three categories: (1) increase in compressive stress caused by disequilibrium compaction and tectonic compression, (2) increase in fluid volume caused by temperature increase, diagenesis, hydrocarbon generation, and cracking to gas, and (3) fluid movement and processes related to density differences between fluids and gases caused by hydraulic head, osmosis, and buoyancy (Osborne and Swarbrick, 1997; Tingay et al., 2009; Zhao et al., 2018).

Conditions that favor disequilibrium compaction are higher sedimentation rates and poor permeability (Bowers, 1995; Osborne and Swarbrick, 1997). The Upper Ordovician is a thick sequence of fine-grained low-permeability sediments, which is an ideal condition for

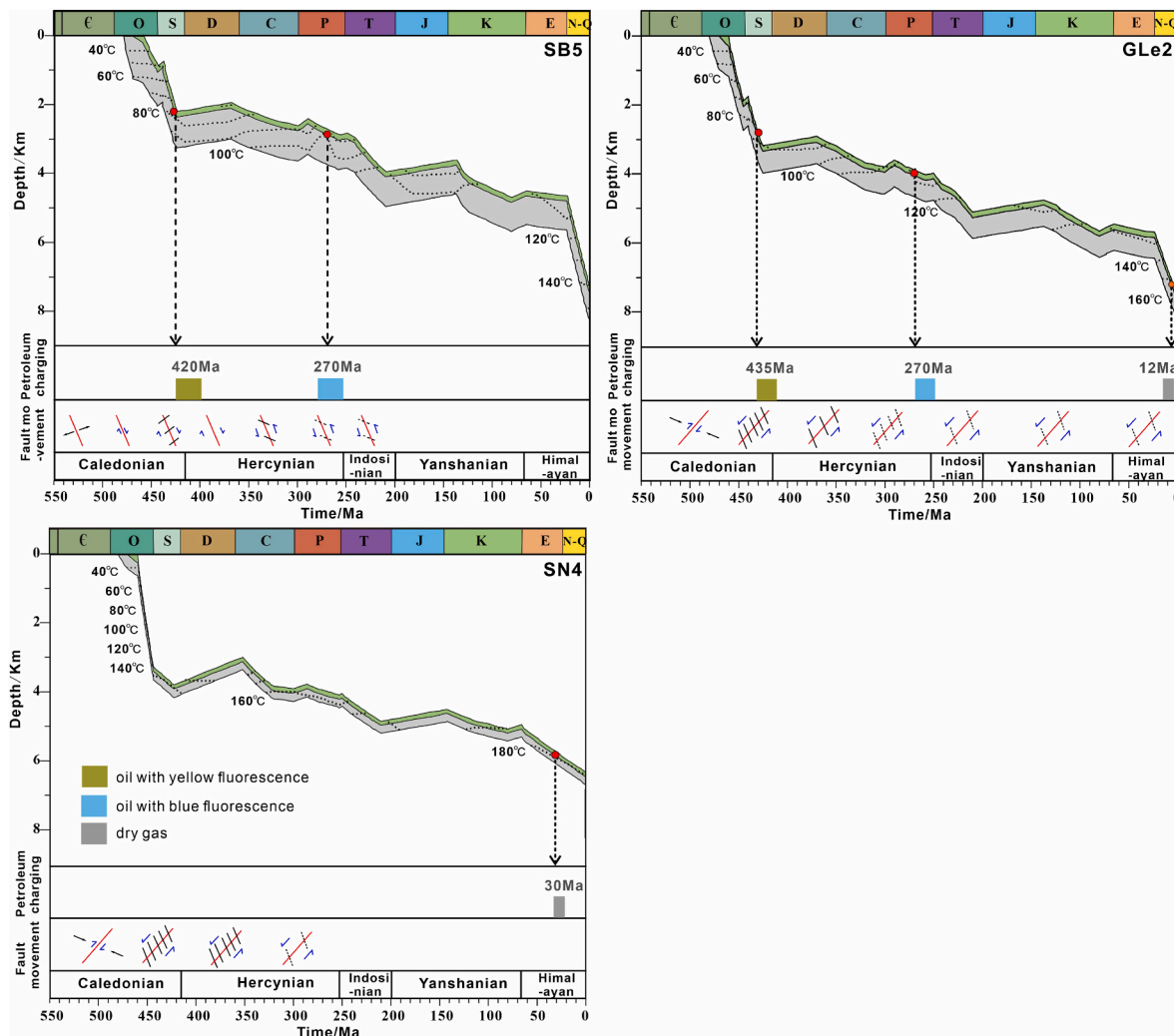


Fig. 11. Burial and thermal history diagram of the Middle-Lower Ordovician reservoirs in the SLU area showing the time of petroleum charging and fault movement in different secondary tectonic units (SB, ST, SN areas). The fault movement is referred to (Yun, 2021), and the minimum homogenization temperature of aqueous inclusions associated with petroleum inclusions is selected to determine petroleum charging time.

Table 3

Compositions of petroleum used to model the pressure, and volume of the Middle-Lower Ordovician petroleum inclusions.

| Mole fraction /% | Well | | | |
|------------------------------|-------|-------|-------|-------|
| Component | SB5 | MS5 | SN4 | GL2 |
| CO ₂ | 0.87 | 1.38 | 13.51 | 4.71 |
| N ₂ | 5.78 | 3.42 | 2.81 | 4.26 |
| C ₁ | 17.36 | 74.00 | 80.91 | 90.74 |
| C ₂ | 7.49 | 9.07 | 1.46 | 0.25 |
| C ₃ | 6.14 | 6.79 | 0.88 | 0.02 |
| iC ₄ | 1.24 | 1.84 | 0.16 | 0.01 |
| nC ₄ | 3.49 | 2.74 | 0.13 | 0.01 |
| iC ₅ | 1.37 | 0.51 | 0.09 | |
| nC ₅ | 2.31 | 0.23 | 0.05 | |
| C ₆ | 3.50 | 0.02 | | |
| C ₇ | 4.74 | | | |
| C ₈ | 5.95 | | | |
| C ₉ | 4.94 | | | |
| C ₁₀ | 4.61 | | | |
| C ₁₁ ⁺ | 30.21 | | | |

C₁=CH₄; C₂=C₂H₆; C₃=C₃H₈; nC₄ = n-butane; iC₄ = isobutane; nC₅ = n-pentane; iC₅ = isopentane; C₆ = hexane; C₇ = heptane; C₈ = octane; C₉ = nonane; C₁₀ = decane; C₁₁⁺ = alkane with C number ≥11.

overpressure generation through disequilibrium compaction. However, when the Upper Ordovician mudstone sequence in the SB area entered the stage of continuous rapid deposition (sedimentation rate of >200 m/Ma) during the Himalayan period, its burial depth was approximately 5 km (Fig. 13). The Upper Ordovician mudstone sequence was too compacted to result in retention of a large amount of pore fluid. Furthermore, the thickness of the Upper Ordovician mudstone layer increases from northwest to southeast, but the Middle-Lower Ordovician reservoirs' high-magnitude overpressures develop mainly in the middle of the SLU area (Figs. 2 and 3). More importantly, the magnitude of overpressure in the Middle-Lower Ordovician carbonates was stronger than that of the overlying Upper Ordovician mudstone strata (Fig. 5). Thus, the high-magnitude overpressure in the Middle-Lower Ordovician reservoir was not derived from the abnormal overpressure in adjacent low permeability mudstone sequence. The SLU area is located in the center of the cratonic region, far away from the orogenic belt. The dip angle of the Middle-Lower Ordovician reservoir does not exceed 3° (Qi, 2016), which suggested the Ordovician formation did not experience any such intensive horizontal shortening that could conceivably generate high-magnitude overpressure. Hence, stress-related mechanisms would not explain the high-magnitude overpressure in the Middle-Lower Ordovician carbonates of the SLU area.

Published studies have quantitatively calculated the magnitude of overpressure formed through several hypothesized fluid expansion

Table 4

Trapping pressure of oil inclusions in the Middle-Lower Ordovician formations.

| Sample | Current depth/m | Th _{oil} /°C | Th _{aqu} /°C | Gas-liquid ratio/% | Paleo-depth/m | Trapping time/Ma | Trapping pressure/MPa | Pressure coefficient |
|--------|-----------------|-----------------------|-----------------------|--------------------|---------------|------------------|-----------------------|----------------------|
| SB5 | 7426.9 | 65.5 | 80.4 | 7.6 | 2200 | 423 | 21.10 | 1.00 |
| | 7426.9 | 63.9 | 103.5 | 6.3 | 2800 | 290 | 27.74 | 1.01 |
| FY1 | 7382.5 | 58.3 | 86.8 | 6.8 | 3035 | 418 | 30.64 | 1.03 |
| | 7382.5 | 72.4 | 113.7 | 8.4 | 4618 | 237 | 50.69 | 1.12 |
| GLe2 | 7388.5 | 80.6 | 109.4 | 11.3 | 3811 | 271.9 | 40.34 | 1.08 |

Th_{oil} = Homogenization temperature of oil inclusion, Th_{aqu} = Homogenization temperature of aqueous inclusion.**Table 5**

Trapping pressure of gas-bearing inclusions in the Middle-Lower Ordovician formations by PVT simulation.

| Sample | Depth/m | Gas-liquid ratio/% | P-T equation | Trapping temperature/°C | Trapping pressure/MPa | Trapping time/Ma | Paleo-depth/m | Pressure coefficient |
|--------|---------|--------------------|-----------------|-------------------------|-----------------------|------------------|---------------|----------------------|
| ST1 | 7860.2 | 9.5 | P = 2.76T-333.6 | 163.0 | 116.28 | 17.5 | 6880 | 1.72 |
| SN1 | 6531.2 | 12.4 | P = 2.56T-343.9 | 163.3 | 74.93 | 15.8 | 6280 | 1.22 |
| SN5 | 6378.0 | 13.0 | P = 2.46T-351.9 | 182.5 | 97.05 | 11.6 | 6072 | 1.63 |
| SN4 | 6361.2 | 12.8 | P = 2.09T-312.4 | 183.8 | 71.74 | 13.5 | 6000 | 1.21 |
| SN501 | 6411.7 | 15.2 | P = 2.37T-354.1 | 183.2 | 79.85 | 8.6 | 6195 | 1.31 |

Table 6

Trapping pressure of gas-bearing inclusions in the Middle-Lower Ordovician formations by Raman shifts and PVT simulation.

| Sample | Depth/m | System | V _{meas} | V _{real} | Gas-liquid ratio/% | Pressure in 25 °C /MPa | Trapping temperature /°C | Trapping pressure /MPa | Trapping time /Ma | Paleo-depth /m | Pressure coefficient |
|--------|---------|-------------------------------------|-------------------|-------------------|--------------------|------------------------|--------------------------|------------------------|-------------------|----------------|----------------------|
| GLe2 | 7386 | CH ₄ -H ₂ O-X | 2916.158 | 2916.243 | 10.2 | 5.29 | 155.2 | 128.8 | 5.3 | 7172 | 1.83 |
| | | | 2916.158 | 2916.435 | 10.6 | 4.61 | 155.2 | 113.8 | 5.3 | 7172 | 1.62 |
| MS5 | 7609 | | 2916.505 | 2916.590 | 12.3 | 4.05 | 158.0 | 78.54 | 11.5 | 6977 | 1.15 |
| | | | 2916.510 | 2916.595 | 12.6 | 4.04 | 158.0 | 74.11 | 11.5 | 6977 | 1.08 |
| GL2 | 5457 | | 2907.720 | 2912.511 | Density 0.20 | / | 148.9 | 53.02 | 30 | 4905 | 1.10 |

X is shown there are other components besides methane and water.

mechanisms under ideal conditions (Luo and Vasseur, 1992; Tremosa et al., 2021; Wangen, 2001). These results indicated that all the proposed fluid expansion mechanisms other than gas generation could contribute only minorly to overpressure formation (Barker, 1990). In addition, the paleo-pressure data collected from several published studies (Chen et al., 2020; Liu et al., 2013, 2019; Lu et al., 2016b; Si et al., 2017) on petroleum inclusions in the Middle-Lower Ordovician reservoirs located in the SLU area and surrounding areas also showed that oil accumulation occurred in reservoir with normal pressure and gas inclusions were formed under overpressured conditions (Fig. 14). The reservoir with overpressure in the SLU area, as shown in Fig. 5, had been produced a large volume of gases during the exploitation, and the gas production corresponds closely with the pressure coefficient of the Middle-Lower Ordovician reservoirs (Fig. 15A and B). Within the limits of the observation, we tentatively suggest that overpressures are primarily generated in the Middle-Lower Ordovician carbonates owing to increase in fluid volume caused by gas generation.

Published studies on kinetics simulation experiments suggested that the threshold temperature for crude oil cracking to gas ranged from 160 °C to 200 °C (Claypool and Mancini, 1989; Horsfield et al., 1992; Pan et al., 2010; Schenk et al., 1997; Waples, 2000). However, high fluid pressure may inhibit the cracking of deep crude oil (Behar and Vandenbroucke, 1996; Dominé and Enguehard, 1992; Hill et al., 1996). No agreement has been arrived upon the threshold temperature for crude oil cracking to gas, which hindered the understanding of the causes of overpressure related to gas generation in the study area. Statistical analysis of reservoir temperature and the gas-to-liquid ratio of many

wells in the SLU area indicated a significant change in the gas-to-liquid volume ratios at a formation temperature of 165 °C–170 °C (Fig. 15C).

The maximum temperature of the Ordovician reservoirs in the ST area was always below 170 °C (Li et al., 2022), which was not high enough to generate massive dry gas by in-situ oil cracking to gas. Therefore, in-situ oil cracking to gas alone cannot explain the strongest overpressure developed in the ST area. Previous geochemical studies suggest that the gas in the ST area was mainly generated by the thermal cracking of kerogen, and crude oil in the Middle-Lower Ordovician formation of well ST1 had the distribution characteristics of n-alkane molar concentration by gas invasion (Chen, 2016; Ma et al., 2021). The present-day temperature of the Middle-Lower Ordovician reservoirs in the SN area was more than 180 °C (Li et al., 2022). Higher dry coefficients (0.95–1.00) and relatively heavy carbon isotopic signatures with average $\delta^{13}\text{C}_1$ and $\delta^{13}\text{C}_2$ values of -36.4‰ and -32.5‰ of nature gases in the SN area, indicated that the nature gases are associated thermogenic gas (Ma et al., 2021; Zhou et al., 2019). However, the absence of large-scale bitumen in the Middle-Lower Ordovician formation indicated that no large-scale oil cracking occurred in the Middle-Lower Ordovician reservoir of the SN area during geological periods (Zhou et al., 2019). The dry gas in the Middle-Lower Ordovician reservoirs of the SN area might not have originated mainly from the in-situ cracking of early charged crude oil but from the cracking gas in deeper petroleum reservoirs. Moreover, the distribution of the highly compartmentalized nature of overpressure is coincident with areas of continuous fault movement (F1, F4, and F8) during the Late Himalayan Period (Figs. 3 and 11). Hence, the upward movement of overpressured

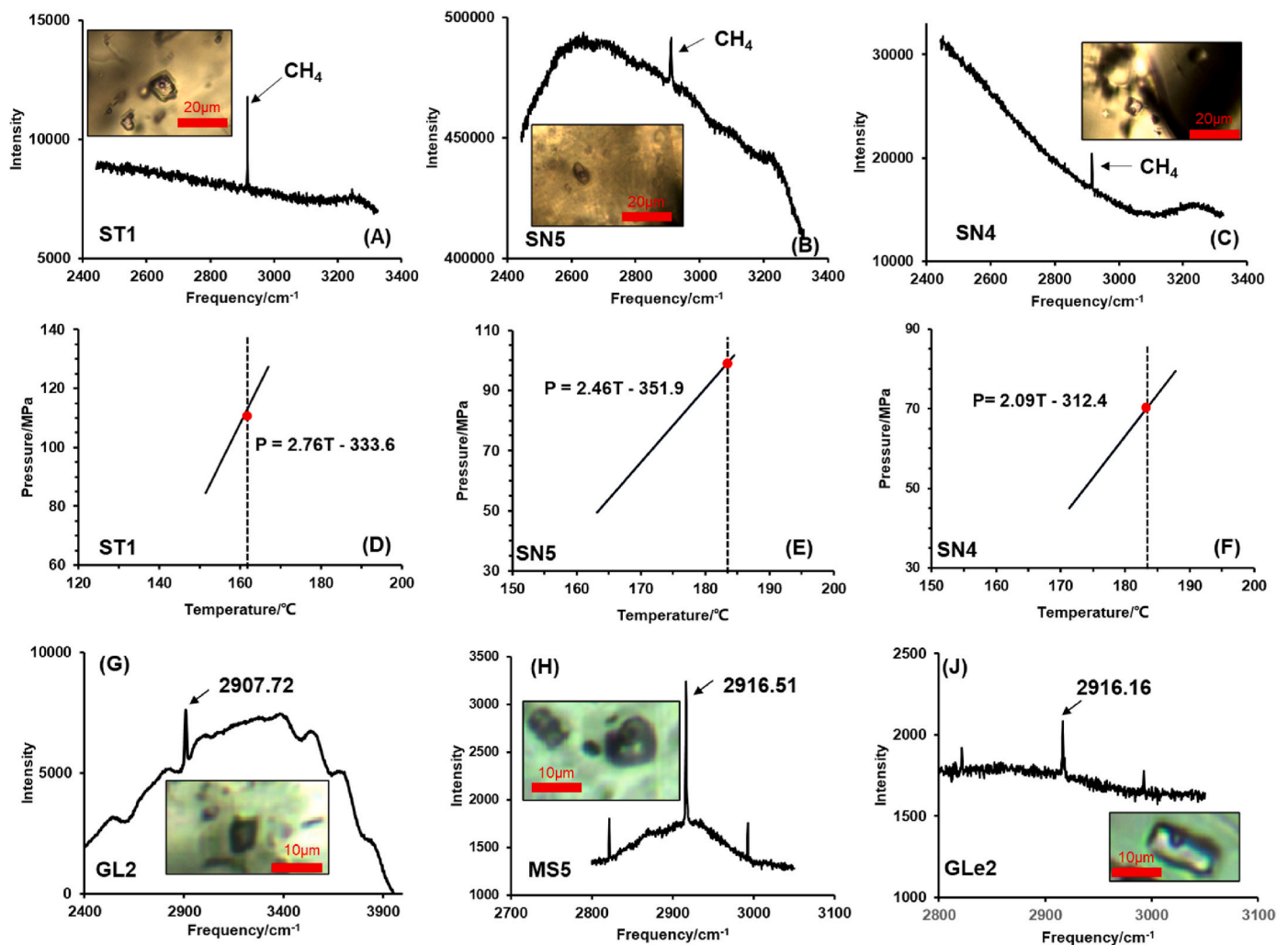


Fig. 12. Raman characteristic peaks of nature gas component in fluid inclusions from six wells (ST1, SN5, SN4, GL2, MS5, GLe2). The P-T lines recovered by methane-bearing aqueous inclusions of Wells ST1, SN5, SN4. The dashed lines represent the homogeneous temperature of coeval aqueous inclusions, and the red dots represent the trapping temperature and pressure of methane-bearing inclusions.

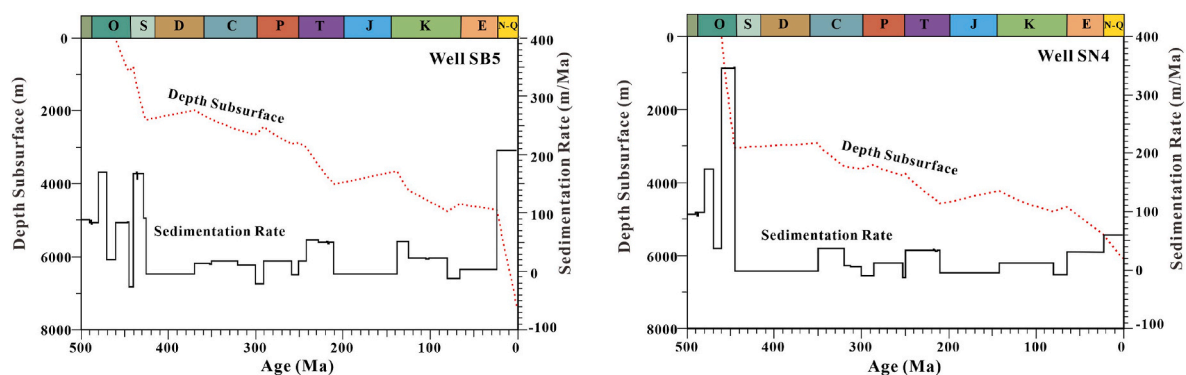


Fig. 13. Sedimentation rates and buried depth of the bottom of the Upper Ordovician shale sequence for wells SB5 and SN4.

gas could lead to significant overpressure in shallow reservoirs through open faults.

5.2. Effect of strike-slip faults on pressure evolution

In the ancient marine carbonate formations, paleo-pressure is key but very difficult to reconstruct (Amrouch et al., 2011; Beaudoin et al.,

2014; Harrison and Summa, 1991; Mello and Karner, 1996). Based on the present-day pressures and paleo-pressures from the fluid inclusion, the pore pressure evolution of Middle-Lower reservoirs was restored by PetroMod2012.1 software. The principle of the software and modelling parameters were previously described in the preceding section. In this study, the aim of the pressure simulation was to show the different overpressure evolution in two types of fault-controlled reservoirs

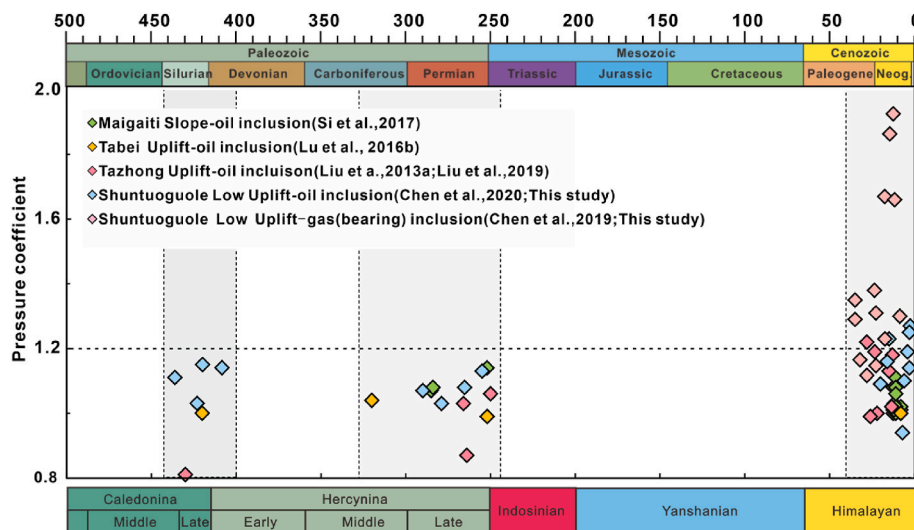


Fig. 14. Schematic diagram of the paleo-pressure coefficient of Middle-Lower Ordovician reservoirs in the Tarim Basin recovered by petroleum inclusions, showing paleo-pressure coefficient of Middle-Lower Ordovician reservoirs during different stages of petroleum accumulation.

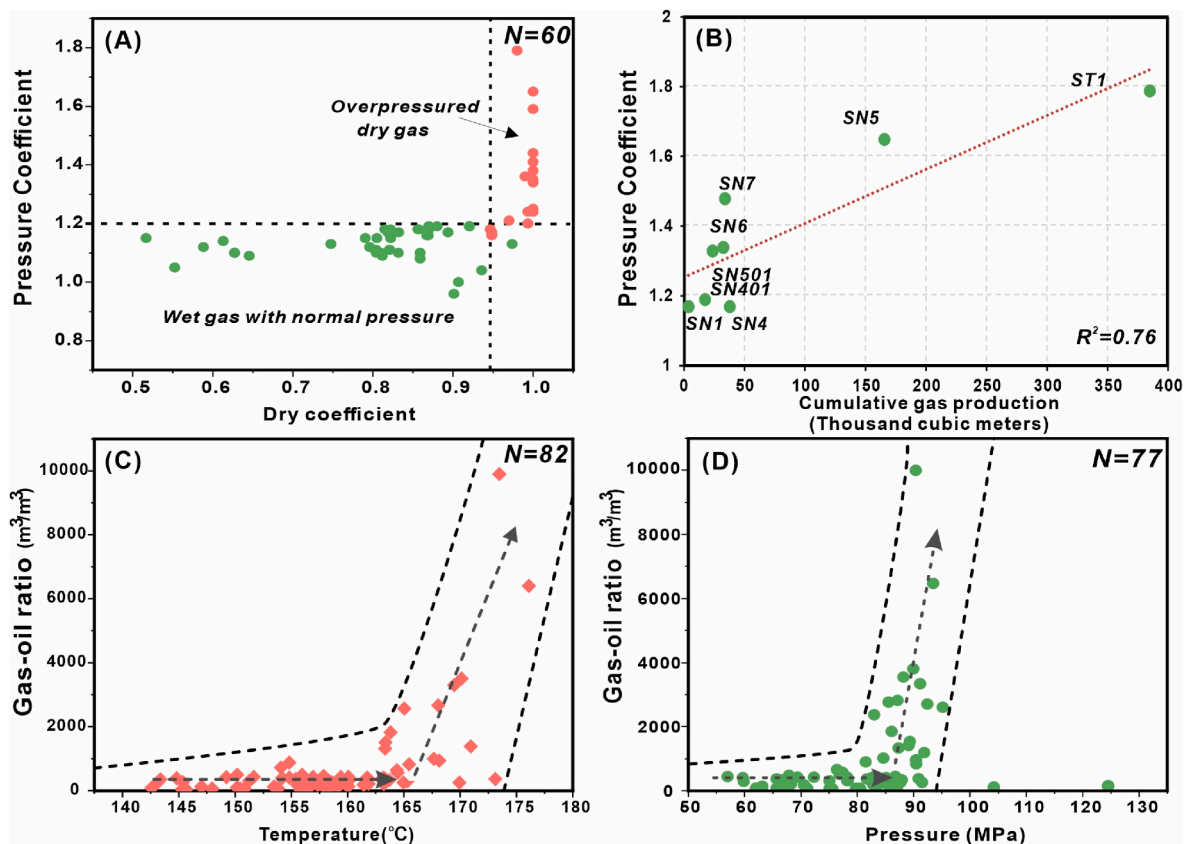


Fig. 15. (A) Crossplot of pressure coefficient vs. dry coefficient. (B) Cross plot of statistical cumulative gas production vs. pressure coefficient. (C) Crossplot of gas-oil ratio vs. temperature. (D) Crossplot of gas-oil ratio vs. pressure. The N represents the number of measured points.

(located either in major fault zones or far away from these fault zones) under the background of petroleum geology.

The pressure evolutionary trend of the two types of reservoirs in wells MS5 and GLE2 was similar before the Himalayan Period but exhibited significant differences in pressure increments during the Himalayan Period (Fig. 16). The Lower Cambrian source rocks in the SLU area entered the hydrocarbon generation threshold and began to generate oil during the Early Ordovician (Li et al., 2022; Qiu et al., 2012). During the

Late Ordovician, the coincidence between the time of the oil window and the stage of intense fault activity led to oil migrating upward from the Cambrian source rock to the Ordovician reservoirs along open major faults. However, oil generation did not always form overpressure in source rock, especially when the proportion of expulsion exceeds 25% (Guo et al., 2012). Therefore, during this stage, oil generation could form only minor residual pressure in Middle-Lower Ordovician reservoirs (Fig. 16).

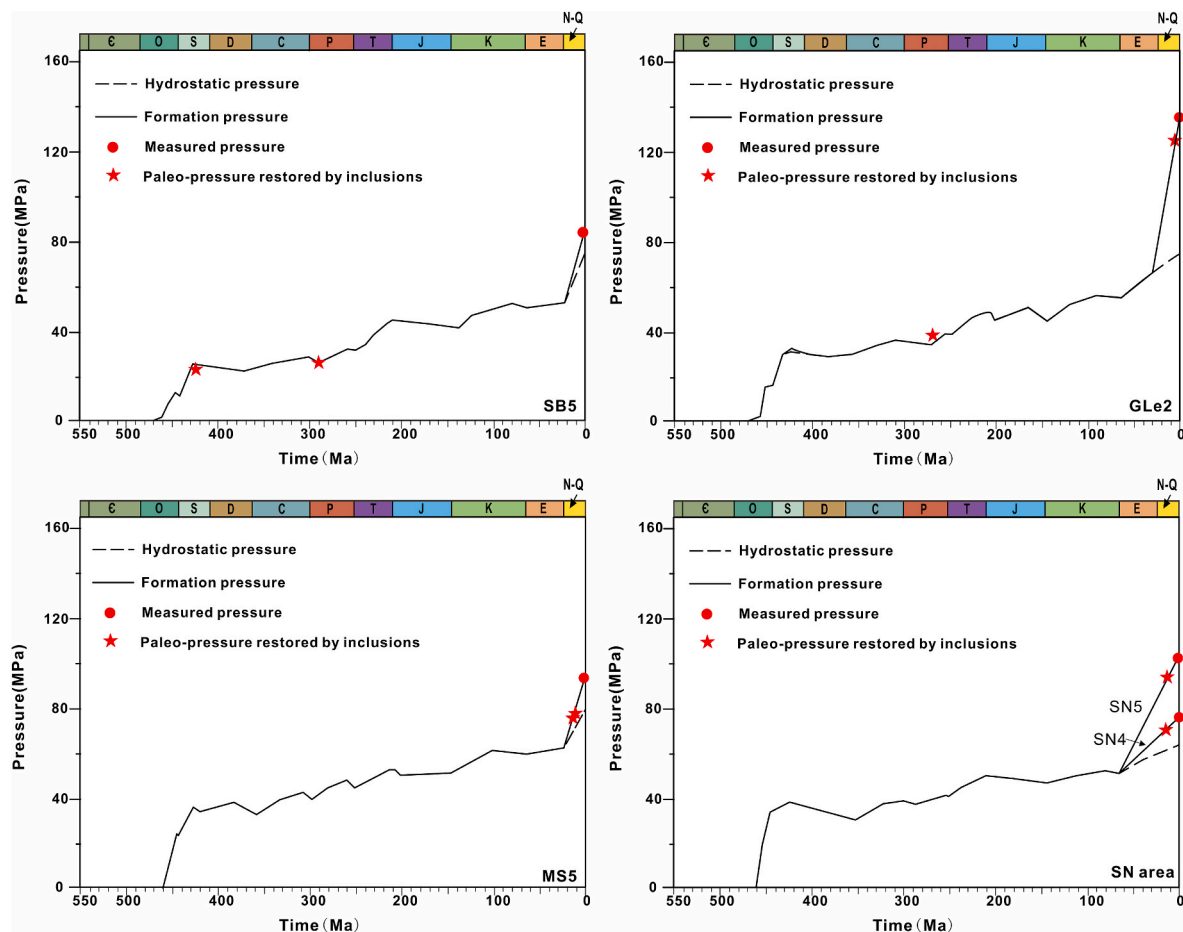


Fig. 16. The pressure evolution of the Middle- Lower Ordovician reservoirs near the major fault (SB5, MS5, SN4) and far from the major fault (GLe2, SN5), showing the discrepant pressure increasing trend in different reservoirs during the Himalayan period. The red stars represent the trapping pressure and time results of hydrocarbon inclusions recovered by the PVT simulation method and Raman shifts method. The red dots are the drilling measured data. The black curves are from basin modelling/burial history analysis.

By the end of the Carboniferous Period, the late mature source rock and the strike-slip fault reactivation enabled the migration of liquids with higher gas-oil ratio condensate oil. When the tectonic movements were relatively strong, strike-slip faulting drove the upward migration of multiple petroleum fluids into the Middle-Lower Ordovician fractured-vuggy reservoirs (Karlsen and Skeie, 2006; Tingay et al., 2009; Yu et al., 2022). However, Oil accumulation was not thought to cause significant changes in fluid pressure in fractured-vuggy reservoirs with high porosity and permeability of well MS5 near the major fault. The relatively poor physical properties made it difficult for oil to migrate into fractured reservoirs, which led to poor levels of oil-bearing and hydrostatic pressures in Middle-Lower Ordovician reservoirs during the Late Caledonian Period and Late Hercynian Period. Therefore, the small volume of oil charging also did not generate excessive residual fluid pressure in the Middle-Lower Ordovician reservoir of well GLe2.

During the Cenozoic Period, the Cambrian source rocks entered the dry gas state (Li et al., 2022; Qiu et al., 2012). During the Himalayan Period, weakly active strike-slip faulting made it difficult to drive the upward migration of fluid. However, overpressure usually drives fluid to move vertically into the overlying lower-pressured sediments (Hunt, 1990; Karlsen and Skeie, 2006). As subsidence progresses and formation temperature increases, the overpressures formed by oil cracking to gas in deeper Cambrian strata provided forces for the vertical migration of gas. Because of the difference in the reservoir's physical properties, dry gas charging led to the build-up of high-magnitude overpressure in the fractured reservoirs (GLe2) but not in the fractured-vuggy reservoirs (MS5). At present, both the burial depth and the temperature of the

Middle-Lower Ordovician reservoir reached their greatest values, as well as fluid pressure (Fig. 16). However, the Middle-Lower Ordovician reservoirs in the SB area's northwest-oriented faults (SB5) have been maintaining normal pressure because of a lack of gas charging (Fig. 16).

Because the present-day temperature of the Middle and Lower Ordovician formation in the SN area is higher than 180 °C (Liu et al., 2020), it is challenging to find reliable oil inclusions to restore paleo-pressure at oil charging. As shown in Fig. 14, oil filling might not generate significant overpressure in the Middle-Lower Ordovician formations of the SLU area, especially when the oil filling amount was not large. Furthermore, the abnormal overpressure generated from early oil accumulation was likely to dissipate because of multi-stage tectonic uplifts in the Caledonian and Hercynian Periods. The pressure evolutionary trend in the fractured reservoirs far away from major faults (SN5) was similar to the fractured-vuggy reservoirs in major fault zones (SN4) in the process before the Himalayan period, and both of them were characterized by normal pressure. The overpressure magnitude of the two types of reservoirs underwent different changes at the stage of gas charging (Fig. 16).

5.3. Effect of strike-slip faults on overpressure distribution

The process of faulting can create not only caves of different sizes, pores, and fractures in deep-buried carbonates along the major faults but also secondary network fractures in damage zones located far from the strike-slip fault (Caine et al., 1996; Cilona et al., 2019; Sibson, 1977). The fracture-cavern assemblages along the strike-slip faults and the

adjacent fractures generally enhanced the bulk porosities and permeabilities in low-porosity carbonates and provided important storage space for hydrocarbon accumulation in low-porosity carbonates (Caine et al., 1996; Deng et al., 2022; Qi, 2020; Sibson, 1977). Recently published studies on the porosity of fault-controlled carbonate reservoirs in the Tarim Basin have emphasized the difference between fractured-vuggy and fractured reservoirs, with porosities ranging from 5% to 45% and from 3% to 8%, respectively (Deng et al., 2022; Ma et al., 2022; Qi, 2020).

Fractured reservoirs have limited storage space and high self-sealing ability when compared with fractured-vuggy reservoirs, which provides a more favorable environment for overpressure generation and preservation. Fractured-vuggy reservoirs are often connected to other cavities through faults (Deng et al., 2022), which have a relieving effect on the increase in fluid overpressure. Hence, strong overpressure created by gas generation develops only in fractured reservoirs located far from major faults, not near the fault zones.

Widespread crack-seal textures and multiperiod secondary inclusions in the cement indicate that pressure pulse associated with subsurface fluid migration may have been episodic (Cox, 2010; Laubach et al., 2004; Ramsay John, 1980; Renard et al., 2006). Most of the fluid activity periods were related to strike-slip activity that corresponded with a structural activity stage (Deng et al., 2022; Li et al., 2023; Yang et al., 2021a; Yu et al., 2022), which indicated that regional structural activity might play an important role in fluid flow in ultra-deep formations of the SLU area. The northwest-oriented strike faults remained inactive after the Late Ordovician Period, and the northeast-oriented strike faults remained continuously active (Yun, 2021). In addition, the trend of northeast-oriented strike-slip fault in the SLU area corresponded to the present-day maximum regional horizontal stress, favoring slip along faults and openness and connection of internal associated fractures between these two first-order major (Deng et al., 2022; Yun, 2021). Open fractures facilitated the upward migration of deep gas along the faults into the Middle-Lower Ordovician reservoirs located far

from the faults of the ST and SN areas and led to overpressure buildup (Fig. 17). However, the continuous activity of northeast-oriented faults in the ST area promoted further opening of the faults and fractures, which promoted more gas to fill into Middle-Lower Ordovician reservoirs and created stronger overpressure than in the SN area. The 20 wells in the study area with more than 1000 tons of oil equivalent per day were all located in the ST area, which confirms that the areas with continuously active faults during the Himalayan Period have more abundant petroleum resources. By contrast, inactive northwest-oriented strike-slip and lower maturity of source rocks could not provide sufficient driving forces for petroleum charging into Middle-Lower Ordovician reservoirs and maintained hydrostatic pressure in the SB area.

The thick mudstone in the Upper Ordovician and stable tectonic environment provided good sealing ability, which facilitated the preservation of the overpressure from the Himalayan Period to the present day. The Cambrian carbonate reservoir, covered by a thick evaporitic rock, is located close to the Yuertusi source rock. There is a higher possibility that the Cambrian carbonate reservoir is filled with large-scale petroleum than the Middle-Lower Ordovician reservoir. Furthermore, the temperature of the Lower Cambrian reservoir in the SLU area has already exceeded the threshold for crude oil cracking. The strong overpressure in the Middle-Lower Ordovician strata transmitted by deep fluid suggests that the unexplored Cambrian reservoir sealed by the evaporitic rock may have overpressure with an even higher magnitude (Fig. 18).

6. Conclusions

Based on comprehensive geological research on the overpressure of Middle-Lower Ordovician reservoirs in the SLU area, the following conclusions can be drawn:

The measured pressure and mud density data of Middle-Lower Ordovician formations show that overpressure developed in the areas located between first-order major faults, but normal pressure generally

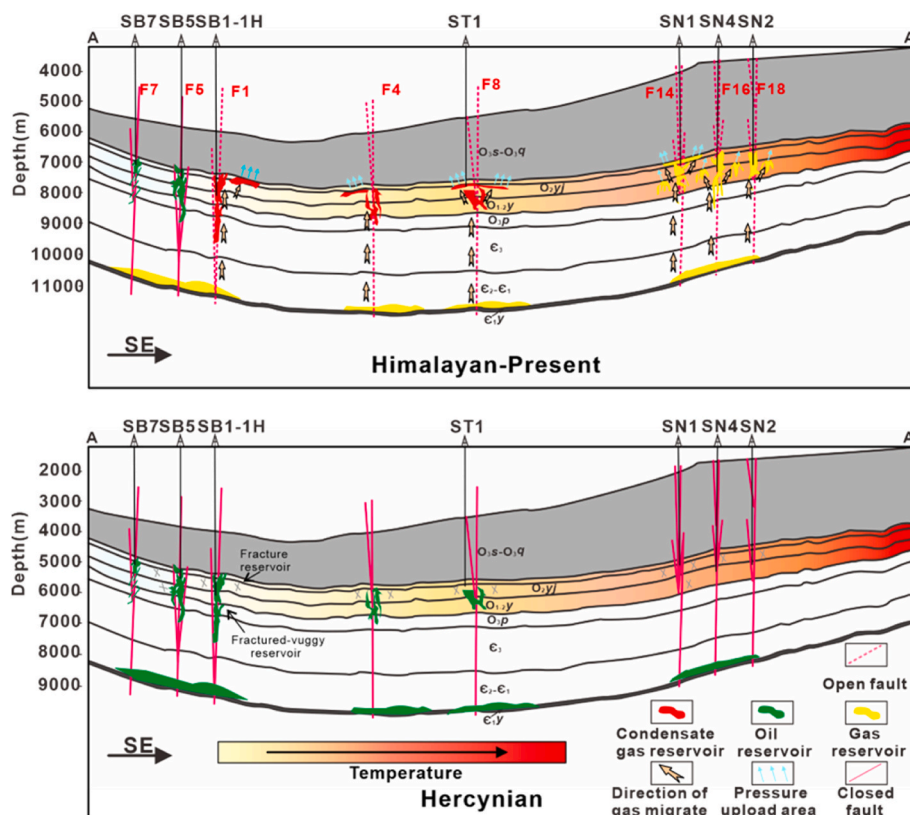


Fig. 17. Schematic illustration of hydrocarbon migration and accumulation in the Shuntuoguole area. The location is shown in Fig. 1.

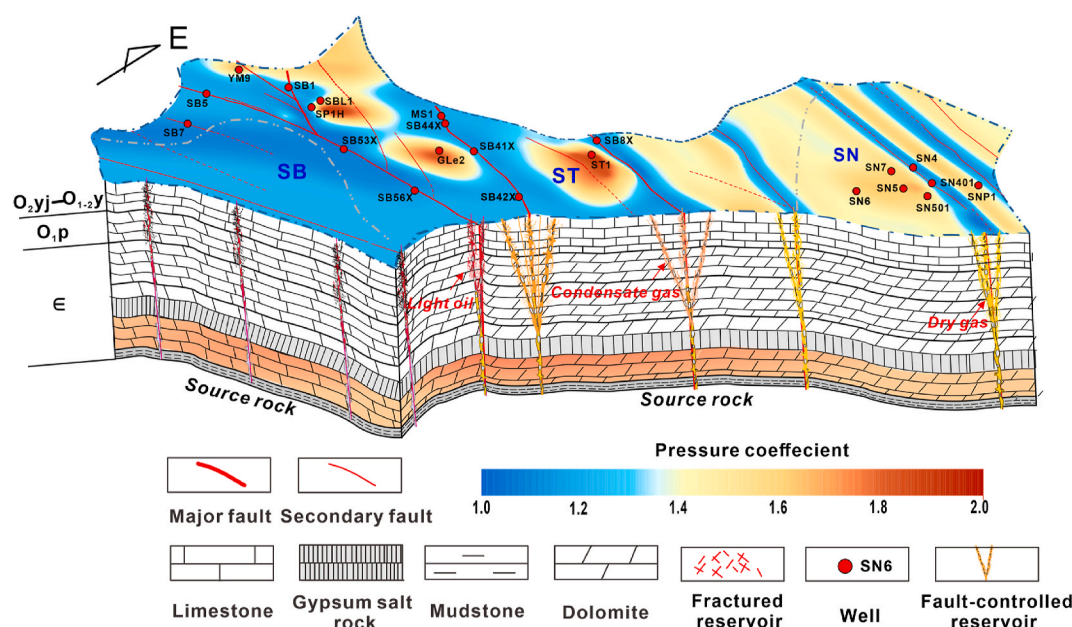


Fig. 18. The distribution pattern of pressure coefficient distribution of ultra-deep carbonate formation in the Shuntuoguole area, Tarim Basin. Deep strong-overpressured fluid under the seal of the Cambrian gypsum rock migrated upward into the Middle-Lower Ordovician reservoir through open faults.

developed in fault zones.

The geological processes and overpressured reservoirs characteristics suggest the overpressure in Middle-Lower Ordovician reservoirs was mainly caused by overpressured gas charging from the Cambrian formations, and the difference in gas accumulation caused by multi-stage fault activity resulted in the compartmentalized distribution pattern of overpressure.

The pressure evolution restored by basin modelling and fluid inclusion indicates that oil accumulation did not form significant paleo-overpressure in two types of reservoirs that are far away from the major faults and around the major faults. The difference in overpressurization between the two types of reservoirs began to be evident at the stage of gas charging.

This study provided a better understanding of the generation and distribution of overpressure in ultra-deep carbonate reservoirs controlled by intra-cratonic strike-slip faults. The results indicate that strike-slip faults not only provide a primary pathway for the migration of overpressured gas from the deeper Cambrian formation into the Middle-Lower Ordovician fault-controlled reservoirs, but also act as barriers to divide the reservoirs into isolated pressure systems. When selecting deep exploration targets, the fractured-vuggy reservoirs with normal pressure that are located in the major strike-slip fault zones may hold great potential for liquid petroleum exploration, while potential overpressure in fractured reservoirs that are located far away from the major strike-slip fault zones should be concerned.

Declaration of competing interest

The authors declare that they have no known competing financial interests or personal relationships that could have appeared to influence the work reported in this paper.

Data availability

Data will be made available on request.

Acknowledgment

The National Natural Science Foundation of China (U19B6003) and

PetroChina Innovation Foundation (2019D-5007-0101) provided financial support. We gratefully acknowledge the Sinopec Northwest Oilfield Company and the PetroChina Tarim Oilfield Company for providing geologic information and core samples.

References

- Amrouch, K., Beaudoin, N., Lacombe, O., Bellahsen, N., Daniel, J.M., 2011. Paleostress magnitudes in folded sedimentary rocks. *Geophys. Res. Lett.* 38, 2–7.
- An, H., Li, H., Wang, J., Du, X., 2009. Tectonic evolution and its controlling on oil and gas accumulation in the northern Tarim Basin. *Geotect. Metallogenia* 33, 142–147.
- Aplin, A., Larter, S., Bigge, M., Macleod, G., Swarbrick, R., Grunberger, D., 2000. PVTX history of the North Sea's Judy oilfield. *J. Geochem. Explor.* 69, 641–644.
- Aplin, A., Macleod, G., Larter, S., Pedersen, K., Sorensen, H., Booth, T., 1999. Combined use of Confocal Laser Scanning Microscopy and PVT simulation for estimating the composition and physical properties of petroleum in fluid inclusions. *Mar. Petrol. Geol.* 16, 97–110.
- Barker, C., 1990. Calculated volume and pressure changes during the thermal cracking of oil to gas in reservoirs. *AAPG (Am. Assoc. Pet. Geol.) Bull.* 74, 1254–1261.
- Bathurst, R.C., 1986. Carbonate diagenesis and reservoir development: conservation, destruction, an creation of pores. *Colorado Sch. Mine. Q.* 81, 1–25.
- Bathurst, R.G., 1972. Carbonate Sediments and Their Diagenesis. Elsevier.
- Beaudoin, N., Lacombe, O., Bellahsen, N., Amrouch, K., Daniel, J.M., 2014. Evolution of pore-fluid pressure during folding and basin contraction in overpressured reservoirs: insights from the Madison-Phosphoria carbonate formations in the Bighorn Basin (Wyoming, USA). *Mar. Petrol. Geol.* 55, 214–229.
- Behar, F., Vandenbroucke, M., 1996. Experimental determination of the rate constants of the n-C25 thermal cracking at 120, 400, and 800 bar: implications for high-pressure/high-temperature prospects. *Energy & Fuels* 10, 932–940.
- Bhullar, A.G., Karlsen, D.A., Backer-Owe, K., Seland, R.T., Le Tran, K., 1999. Dating reservoir filling—a case history from the North Sea. *Mar. Petrol. Geol.* 16, 581–603.
- Bourdet, J., Pironon, J., Levresse, G., Tritlla, J., 2008. Petroleum type determination through homogenization temperature and vapour volume fraction measurements in fluid inclusions. *Geofluids* 8, 46–59.
- Bowers, G.L., 1995. Pore pressure estimation from velocity data: accounting for overpressure mechanisms besides undercompaction. *SPE Drill. Complet.* 10, 89–95.
- Burnham, A.K., Sweeney, J.J., 1989. A chemical kinetic model of vitrinite maturation and reflectance. *Geochem. Cosmochim. Acta* 53, 2649–2657.
- Byerlee, J., 2013. Friction, overpressure and fault normal compression. *Geophys. Res. Lett.* 17, 2109–2112.
- Caine, J.S., Evans, J.P., Forster, C.B., 1996. Fault zone architecture and permeability structure. *Geology* 24, 1025–1028.
- Carver, R.E., 1968. Differential compaction as a cause of regional contemporaneous faults. *AAPG (Am. Assoc. Pet. Geol.) Bull.* 52, 414–419.
- Caumon, M.-C., Robert, P., Laverret, E., Tarantola, A., Randi, A., Pironon, J., Dubessy, J., Girard, J.-P., 2014. Determination of methane content in NaCl–H₂O fluid inclusions by Raman spectroscopy. Calibration and application to the external part of the Central Alps (Switzerland). *Chem. Geol.* 378, 52–61.
- Chen, J., 2016. Genetic Mechanism of Marine Hydrocarbons in Western Tazhong. China University of Petroleum (Beijing), Beijing.

- Chen, Q., Xi, B., Han, J., Xu, J., Wu, X., Zhu, X., Ma, Z., 2020. Preservation and influencing factors of ultra-deep oil reservoirs in the Shuntuoguole area, Tarim Basin: evidence from fluid inclusions. *China Petroleum Exploration* 25, 121–133.
- Cilona, A., Solum, J.G., Lucca, A., Storti, F., Taberner, C., 2019. Evolution of Pore Types and Petrophysical Properties of Fault Rocks in Low-Porosity Carbonates, vol. 112. SEPM Special Publications.
- Claypool, G.E., Mancini, E.A., 1989. Geochemical relationships of petroleum in Mesozoic reservoirs to carbonate source rocks of Jurassic Smackover Formation, southwestern Alabama. *AAPG (Am. Assoc. Pet. Geol.) Bull.* 73, 904–924.
- Cox, S.F., 2010. The application of failure mode diagrams for exploring the roles of fluid pressure and stress states in controlling styles of fracture-controlled permeability enhancement in faults and shear zones. *Geofluids* 10, 217–233.
- Croize, D., Renard, F., Gratier, J.-P., 2013. Compaction and porosity reduction in carbonates: a review of observations, theory, and experiments. *Adv. Geophys.* 54, 181–238.
- Darby, D., Funnell, R.H., 2001. Overpressure associated with a convergent plate margin: east Coast Basin, New Zealand. *Petrol. Geosci.* 7, 291–299.
- Deng, S., Li, H., Zhang, Z., Zhang, J., Yang, X., 2019. Structural characterization of intracratonic strike-slip faults in the central Tarim Basin. *AAPG (Am. Assoc. Pet. Geol.) Bull.* 103, 109–137.
- Deng, S., Zhao, R., Kong, Q., Li, Y., Li, B., 2022. Two distinct strike-slip fault networks in the Shunbei area and its surroundings, Tarim Basin: hydrocarbon accumulation, distribution, and controlling factors. *AAPG (Am. Assoc. Pet. Geol.) Bull.* 106, 77–102.
- Dickey, P.A., Shiram, C.R., Paine, W.R., 1968. Abnormal Pressures in Deep Wells of Southwestern Louisiana: high fluid pressures are associated with slump-type faults and shed light on processes of compaction. *Science* 160, 609–615.
- Dominé, F., Enguehard, F., 1992. Kinetics of hexane pyrolysis at very high pressures—3. Application to geochemical modeling. *Org. Geochem.* 18, 41–49.
- Drews, M.C., Bauer, W., Caracciolo, L., Stollhofen, H., 2018. Disequilibrium compaction overpressure in shales of the Bavarian Foreland Molasse Basin: results and geographical distribution from velocity-based analyses. *Mar. Petrol. Geol.* 92, 37–50.
- Duan, Z.H., Moller, N., Weare, J.H., 1992. An equation of state for the CH₄-CO₂-H₂O system: I. Pure systems from 0 to 1000 °C and 0 to 8000 bar. *Geochimica et Cosmochimica acta* 56, 2605–2617.
- Dubessy, J., Buschaert, S., Lamb, W., Pironon, J., Thiéry, R., 2001. Methane-bearing aqueous fluid inclusions: Raman analysis, thermodynamic modelling and application to petroleum basins. *Chem. Geol.* 173, 193–205.
- Eaton, B.A., 1972. The effect of overburden stress on geopressure prediction from well logs. *J. Petrol. Technol.* 24, 929–934.
- Fabre, D., Couty, R., 1986. Etude, par spectroscopie Raman, du méthane comprimé jusqu'à 3 kbar. Application à la mesure de pression dans les inclusions fluides contenues dans les minéraux. *Comptes rendus de l'Académie des sciences. Série 2, Mécanique, Physique, Chimie, Sciences de l'univers, Sciences de la Terre.* 303, 1305–1308.
- Fillippone, W., 1979. On the Prediction of Abnormally Pressured Sedimentary Rocks from Seismic Data. Offshore Technology Conference, OnePetro.
- Gao, J., He, S., Zhao, J.-x., Yi, J., 2017. Geothermometry and geobarometry of overpressured lower Paleozoic gas shales in the Jiaoshiba field, Central China: insight from fluid inclusions in fracture cements. *Mar. Petrol. Geol.* 83, 124–139.
- Goldstein, R.H., Reynolds, T.J., 1994. Systematics of Fluid Inclusions in Diagenetic Minerals. SEPM Society for Sedimentary Geology.
- Grauls, D.J., Baleix, J.M., 1994. Role of overpressures and in situ stresses in fault-controlled hydrocarbon migration: a case study. *Mar. Petrol. Geol.* 11, 734–742.
- Green, S., O'Connor, S.A., Edwards, A., 2016. Predicting Pore Pressure in Carbonates: a Review. *Search and Discovery Article# 41830*.
- Guo, X., He, S., Liu, K., Zheng, L., 2012. Quantitative estimation of overpressure caused by oil generation in petroliferous basins. *Org. Geochem.* 42, 1343–1350.
- Guo, X., Liu, K., Jia, C., Song, Y., Zhao, M., Zhuo, Q., Lu, X., 2016. Constraining tectonic compression processes by reservoir pressure evolution: overpressure generation and evolution in the Kelasu Thrust Belt of Kuqa Foreland Basin, NW China. *Mar. Petrol. Geol.* 72, 30–44.
- Han, X., Deng, S., Tang, L., Cao, Z., 2017. Geometry, kinematics and displacement characteristics of strike-slip faults in the northern slope of Tazhong uplift in Tarim Basin: a study based on 3D seismic data. *Mar. Petrol. Geol.* 88, 410–427.
- Hantschel, T., Kauerauf, A.I., 2009. Fundamentals of Basin and Petroleum Systems Modeling. Springer Science & Business Media.
- Harrison, W.J., Summa, L.L., 1991. Paleohydrology of the gulf of Mexico basin. *Am. J. Sci.* 291, 109–176.
- Hill, R.J., Tang, Y., Kaplan, I.R., Jenden, P.D., 1996. The influence of pressure on the thermal cracking of oil. *Energy & Fuels* 10, 873–882.
- Horsfield, B., Schenk, H.J., Mills, N., Welte, D.H., 1992. An investigation of the in-reservoir conversion of oil to gas: compositional and kinetic findings from closed-system programmed-temperature pyrolysis. *Org. Geochem.* 19, 191–204.
- Jia, C., 2004. Episodes and geodynamic setting of Himalayan movement in China. *Oil Gas Geol.* 02, 121–125+169.
- Hunt, J.M., 1990. Generation and migration of petroleum from abnormally pressured fluid compartments. *AAPG Bull.* 74, 1–12.
- Jia, C., Ma, D., Yuan, J., Wei, G., Yang, M., Yan, L., Tian, F., Jiang, L., 2022. Structural characteristics, formation & evolution and genetic mechanisms of strike-slip faults in the Tarim Basin. *Nat. Gas. Ind. B* 9, 51–62.
- Jiao, F., 2017. Significance of oil and gas exploration in NE strike-slip fault belts in Shuntuoguole area of Tarim Basin. *Oil Gas Geol.* 38, 831–839.
- Karlsen, D.A., Nedkvitne, T., Larter, S.R., Bjørlykke, K., 1993. Hydrocarbon composition of authigenic inclusions: application to elucidation of petroleum reservoir filling history. *Geochem. Cosmochim. Acta* 57, 3641–3659.
- Karlsen, D.A., Skeie, J.E., 2006. Petroleum migration, faults and overpressure, Part I: calibrating basin modelling using petroleum in traps - a review. *J. Petrol. Geol.* 29, 227–256.
- Karthikeyan, G., Dutta, J., Kumar, A., Bhardwaj, N., Sinha, N., 2020. Fault-Related overpressure in the Krishna-Godavari basin, India. *Interpretation* 8, T183–T193.
- Larson, L., Miller, J., Nadeau, J., Roedder, E., 1973. Two sources of error in low temperature inclusion homogenization determination, and corrections on published temperatures for the East Tennessee and Laisvall deposits. *Econ. Geol.* 68, 113–116.
- Laubach, S.E., Olson, J.E., Gale, J.F.W., 2004. Are open fractures necessarily aligned with maximum horizontal stress? *Earth Planet Sci. Lett.* 222, 191–195.
- Lee, J., Swarbrick, R., O'Connor, S., 2022. Kicks and their significance in pore pressure prediction. *Petrol. Geosci.* 28, petgeo2021–061.
- Li, D., Chang, J., Qiu, N., Wang, J., Zhang, M., Wu, X., Han, J., Li, H., Ma, A., 2022. The thermal history in sedimentary basins: a case study of the central Tarim Basin, Western China. *J. Asian Earth Sci.* 229, 105149.
- Li, H., Gao, J., Cao, Z., Zhu, X., Guo, X., Zeng, S., 2023. Spatial-temporal distribution of fluid activity and hydrocarbon accumulation significance in the strike-slip fault zones of Shuntuoguole low-uplift in Tarim Basin. *Earth Sci. Front.* 1–13.
- Lin, F., Bodnar, R., Becker, S., 2007. Experimental determination of the Raman CH₄ symmetric stretching (ν_1) band position from 1–650 bar and 0.3–22 °C: Application to fluid inclusion studies. *Geochem. Cosmochim. Acta* 71, 3746–3756.
- Liu, K., Bourdet, J., Zhang, B., Zhang, N., Lu, X., Liu, S., Pang, H., Li, Z., Guo, X., 2013. Hydrocarbon charge history of the Tazhong Ordovician reservoirs, Tarim Basin as revealed from an integrated fluid inclusion study. *Petrol. Explor. Dev.* 40, 183–193.
- Liu, K., Xiao, X., Mills, D., George, S.C., Volk, H., Gong, S., 2009. Cautions in the interpretation of petroleum fluid inclusion data in petroleum system analysis: insight from spectroscopic analyses of natural and synthetic inclusions. *J. Geochem. Explor.* 101, pp. 62–62.
- Liu, W., Qiu, N., Xu, Q., Liu, Y., Shen, A., Zhang, G., 2018. The evolution of pore-fluid pressure and its causes in the Sinian-Cambrian deep carbonate gas reservoirs in central Sichuan Basin, southwestern China. *J. Pet. Sci. Eng.* 169, 96–109.
- Liu, Y., Qiu, N., Chang, J., Jia, J., Li, H., Ma, A., 2020. Application of clumped isotope thermometry to thermal evolution of sedimentary basins: a case study of Shuntuoguole area in Tarim Basin. *Chin. J. Geophys.* 63, 597–611.
- Liu, Y., Qiu, N., Hu, W., Li, H., Shen, F., Yao, Q., 2019. Temperature and pressure characteristics of Ordovician gas condensate reservoirs in the Tazhong area, Tarim Basin, northwestern China. *AAPG (Am. Assoc. Pet. Geol.) Bull.* 103, 1351–1381.
- Liu, Y., Suppe, J., Cao, Y., Hao, F., Liu, Y., Wang, X., Wu, K., Cao, Z., Wei, H., 2023. Linkage and formation of strike-slip faults in deep basins and the implications for petroleum accumulation: a case study from the Shunbei area of the Tarim Basin, China. *AAPG (Am. Assoc. Pet. Geol.) Bull.* 107, 331–355.
- Lu, W., Chou, L.-M., Burruss, R., Song, Y., 2007a. A unified equation for calculating methane vapor pressures in the CH₄-H₂O system with measured Raman shifts. *Geochem. Cosmochim. Acta* 71, 3969–3978.
- Lu, W., Chou, L.M., Burruss, R.C., Song, Y., 2007b. A unified equation for calculating methane vapor pressures in the CH₄-H₂O system with measured Raman shifts. *Geochem. Cosmochim. Acta* 71, 3969–3978.
- Lu, X., Liu, K., Zhao, M., Zhang, B., Yang, C., Fan, J., Li, X., 2016a. Accumulation Mechanism Analysis of the Typical Deep Reservoirs in Tarim Basin. *Journal of Northeast Petroleum University*.
- Lu, X., Liu, K., Zhao, M., Zhang, B., Yang, C., Fan, J., Li, X., 2016b. Accumulation mechanism analysis of the typical deep reservoirs in Tarim basin. *Journal of Northeast Petroleum University* 40, 62–73+68.
- Lubanzadio, M., Goutly, N., Swarbrick, R., 2002. Variation of velocity with effective stress in chalk: null result from North Sea well data. *Mar. Petrol. Geol.* 19, 921–927.
- Luo, X., Dong, W., Yang, J., Yang, W., 2003. Overpressuring mechanisms in the Yinggehai basin, south China sea. *AAPG (Am. Assoc. Pet. Geol.) Bull.* 87, 629–645.
- Luo, X., Vasseur, G., 1992. Contributions of compaction and aquathermal pressuring to geopressure and the influence of environmental conditions. *AAPG Bull.* 76, 1550–1559.
- Luo, X., Wang, Z., Zhang, L., Yang, W., Liu, L., 2007. Overpressure generation and evolution in a compressional tectonic setting, the southern margin of Junggar Basin, northwestern China. *AAPG (Am. Assoc. Pet. Geol.) Bull.* 91, 1123–1139.
- Ma, A., He, Z., Yun, L., Wu, X., Qiu, N., Chang, J., Lin, H., Cao, Z., Zhu, X., You, D., 2021. The geochemical characteristics and origin of Ordovician ultra-deep natural gas in the North Shuntuoguole area, Tarim Basin, NW China. *Journal of Natural Gas Geoscience* 6, 289–300.
- Ma, Q., Sha, X., Li, Y., Zhu, X., Yang, S., Li, H., 2012. Characteristics of strike-slip fault and its controlling on oil in Shuntuoguole region, middle Tarim Basin. *Petroleum Geology & Experiment* 34, 120–124.
- Ma, Y., Cai, X., Yun, L., Li, Z., Li, H., Deng, S., Zhao, P., 2022. Practice and theoretical and technical progress in exploration and development of Shunbei ultra-deep carbonate oil and gas field, Tarim Basin, NW China. *Petrol. Explor. Dev.* 49, 1–20.
- Madon, M., 2007. Overpressure development in rift basins: an example from the Malay Basin, offshore Peninsular Malaysia. *Petrol. Geosci.* 13, 169–180.
- Mallon, A., Swarbrick, R., 2008. Diagenetic characteristics of low permeability, non-reservoir chalks from the Central North Sea. *Mar. Petrol. Geol.* 25, 1097–1108.
- Matapour, Z., Karlsen, D., 2017. Geochemical characteristics of the Skrugard oil discovery, Barents Sea, Arctic Norway: a “palaeo-biodegraded-gas reactivated” hydrocarbon accumulation. *J. Petrol. Geol.* 40, 125–152.
- Matapour, Z., Karlsen, D., Lerch, B., Backer-Owe, K., 2019. Petroleum occurrences in the carbonate lithologies of the gohta and alta discoveries in the barents sea, arctic Norway. *Petrol. Geosci.* 25, 50–70.
- Mazzullo, S., Harris, P., 1991. An Overview of Dissolution Porosity Development in the Deep-Burial Environment, with Examples from Carbonate Reservoirs in the Permian Basin. *West Texas Geological Society, Midland, TX*, 91–89.

- McLimens, R.K., 1987. The application of fluid inclusions to migration of oil and diagenesis in petroleum reservoirs. *Appl. Geochem.* 2, 585–603.
- Mello, U.T., Karner, G.D., 1996. Development of sediment overpressure and its effect on thermal maturation: application to the Gulf of Mexico basin. *AAPG Bull.* 80, 1367–1396.
- Mohamad, R., Fadipe, O., Zhang, X., Djuraev, O., MacGregor, A., Bouhlef, A., Koutsabeloulis, N., Noufal, A., Sirat, M., Popa, D., 2015. Prediction of Carbonate Reservoirs Pore Pressure and Porosity in Onshore Abu Dhabi Using Petroleum Systems Modeling Technology, Abu Dhabi International Petroleum Exhibition and Conference. OnePetro.
- Mullis, J., 1979. The system methane-water as a geologic thermometer and barometer from the external part of the Central Alps. *Bull. Mineral.* 102, 526–536.
- Nedkvitne, T., Karlsen, D.A., Bjørlykke, K., Larter, S.R., 1993. Relationship between reservoir diagenetic evolution and petroleum emplacement in the Ula Field, North Sea. *Mar. Petrol. Geol.* 10, 255–270.
- Osborne, M.J., Swarbrick, R.E., 1997. Mechanisms for generating overpressure in sedimentary basins: a reevaluation. *AAPG (Am. Assoc. Pet. Geol.) Bull.* 81, 1023–1041.
- Ozkale, A., 2007. Overpressure Prediction by Mean Total Stress Estimate Using Well Logs for Compressional Environments with Strike-Slip or Reverse Faulting Stress State. Texas A&M University.
- Pan, C., Jiang, L., Liu, J., Zhang, S., Zhu, G., 2010. The effects of calcite and montmorillonite on oil cracking in confined pyrolysis experiments. *Org. Geochem.* 41, 611–626.
- Peacock, D.C., Tarnelli, E., Anderson, M.W., 2017. Interplay between stress permutations and overpressure to cause strike-slip faulting during tectonic inversion. *Terra Nova* 29, 61–70.
- Pironon, J., Bourdet, J., 2008. Petroleum and aqueous inclusions from deeply buried reservoirs: experimental simulations and consequences for overpressure estimates. *Geochem. Cosmochim. Acta* 72, 4916–4928.
- Prezbindowski, D.R., Larese, R.E., 1987. Experimental stretching of fluid inclusions in calcite—implications for diagenetic studies. *Geology* 15, 333–336.
- Qi, L., 2016. Oil and gas breakthrough in ultra-deep Ordovician carbonate formations in Shuntuoguole uplift, Tarim Basin. *China Petroleum Exploration* 21, 38–51.
- Qi, L., 2020. Characteristics and inspiration of ultra-deep fault-karst reservoir in the Shunbei area of the Tarim Basin. *China Petroleum Exploration* 25, 102–111.
- Qiu, N., Chang, J., Zuo, Y., Wang, J., Li, H., 2012. Thermal evolution and maturation of lower Paleozoic source rocks in the Tarim Basin, northwest China. *AAPG Bull.* 96, 789–821.
- Radwan, A.E., 2022. A multi-proxy approach to detect the pore pressure and the origin of overpressure in sedimentary basins: an example from the Gulf of Suez rift basin. *Front. Earth Sci.* 10, 967201.
- Ramsay John, G., 1980. The crack-seal mechanism of rock deformation. *Nature* 284, 135–139.
- Renard, F., Andréani, M., Boullier, A.M., Labaume, P., 2006. Crack-seal patterns: records of uncorrelated stress release variations in crustal rocks. *Geological Society London Special Publications* 243, 81–95.
- Rice, J.R., 1992. Fault Stress States, Pore Pressure Distributions, and the Weakness of the San Andreas Fault. *International Geophysics* 51, 475–503.
- Roedder, E., 1972. Composition of Fluid Inclusions.
- Ryder, A.G., 2005. Analysis of crude petroleum oils using fluorescence spectroscopy, *Reviews in Fluorescence* 2005. Springer 169–198.
- Schenck, H.J., Primio, R.D., Horsfield, B., 1997. The conversion of oil into gas in petroleum reservoirs. Part 1: comparative kinetic investigation of gas generation from crude oils of lacustrine, marine and fluviodeltaic origin by programmed-temperature closed-system pyrolysis. *Org. Geochem.* 26, 467–481.
- Si, S., Chen, H., Li, C., Li, P., Chen, X., 2017. Paleo-pressure of fluid inclusion in the yingshan formation reservoirs of the manan structural belt, maigaiti slope. *Geol. J. China Univ.* 23, 706–714.
- Sibson, R.H., 1977. Fault rock and fault mechanisms. *J. Geol. Soc.* 133, 191–213.
- Stasiuk, L., Snowdon, L., 1997. Fluorescence micro-spectrometry of synthetic and natural hydrocarbon fluid inclusions: crude oil chemistry, density and application to petroleum migration. *Appl. Geochem.* 12, 229–241.
- Sun, L., 2003. Development of Gas Condensate Fields in the Tarim Basin. Petroleum Industry Press.
- Swarbrick, R.E., 2001. Challenges of Porosity Based Pore Pressure Prediction, 63rd EAGE Conference & Exhibition. EAGE Publications BV cp-15-00068.
- Swarbrick, R.E., Lahann, R.W., 2016. Estimating pore fluid pressure-stress coupling. *Mar. Petrol. Geol.* 78, 562–574.
- Sweeney, J.J., Burnham, A.K., 1990. Evaluation of a simple model of vitrinite reflectance based on chemical kinetics. *AAPG Bull.* 74, 1559–1570.
- Tingay, M., Hillis, R.R., Swarbrick, R.E., 2009. Origin of overpressure and pore-pressure prediction in the Baram province, Brunei. *AAPG (Am. Assoc. Pet. Geol.) Bull.* 93, 51–74.
- Tremosa, J., Gaucher, E.C., Gailhanou, H., 2021. Overpressure generation by smectite dehydration in sedimentary basins constrained by salinity dilution and stable isotopes. *Appl. Geochem.* 131, 105035.
- Wang, M., Ye, D., 1998. Distribution of formation pressure and the relation with hydrocarbon in northern tarim basin. *Xinjiang Petroleum Geology* 2, 29–33+88.
- Wang, Z., Gao, Z., Fan, T., Zhang, H., Yuan, Y., Wei, D., Qi, L., Yun, L., Karubandika, G. M., 2022. Architecture of strike-slip fault zones in the central Tarim Basin and implications for their control on petroleum systems. *J. Petrol. Sci. Eng.* 213, 110432.
- Wangen, M., 2001. A quantitative comparison of some mechanisms generating overpressure in sedimentary basins. *Tectonophysics* 334, 211–234.
- Waples, D.W., 2000. The kinetics of in-reservoir oil destruction and gas formation: constraints from experimental and empirical data, and from thermodynamics. *Org. Geochem.* 31, 553–575.
- Warner, E.M., 1998. Structural Geology and Pressure Compartmentalization of Jonah Field, Sublette County, Wyoming.
- Webster, M., O'Connor, S., Pindar, B., Swarbrick, R., 2011. Overpressures in the taranaki basin: distribution, causes, and implications for exploration. *AAPG Bull.* 95, 339–370.
- Wei, G., Zhu, Y., Zheng, J., Guang, Y.U., Xinfeng, N.I., Yan, L., Tian, L., Huang, L., 2021. Tectonic-lithofacies paleogeography, large-scale source-reservoir distribution and exploration zones of Cambrian subsalt formation, Tarim Basin, NW China. *Petrol. Explor. Dev.* 48, 1114–1126.
- Weller, J.M., 1959. Compaction of sediments. *AAPG (Am. Assoc. Pet. Geol.) Bull.* 43, 273–310.
- Wu, G., Deng, W., Huang, S., Zheng, D., Pan, W., 2020a. Tectonic-paleogeographic evolution in the Tarim Basin. *Chinese Journal of Geology* 55, 17.
- Wu, G., Ma, B., HanJianfa Guan, B., Chen, X., Yang, P., Xie, Z., 2021. Origin and growth mechanisms of strike-slip faults in the central Tarim cratonic basin, NW China. *Petrol. Explor. Dev.* 48, 595–607.
- Wu, G., Yang, H., Qu, T., Li, H., Luo, C., Li, B., 2012. The fault system characteristics and its controlling roles on marine carbonate hydrocarbon in the Central uplift, Tarim basin. *Acta Petrol. Sin.* 28, 793–805.
- Wu, G., Zhang, T., Zhu, Y., Wan, X., Chang, X., 2020b. The architecture, distribution and growth of carbonate fault damage zone. *Chinese Journal of Geology* 55, 68–80.
- Xu, Z., Li, S., Zhang, J., Yang, J., Cai, Z., 2011. Paleo-Asian and Tethyan tectonic systems with docking the Tarim block. *Acta Petrol. Sin.* 27, 1–22.
- Yang, H., Wu, G., Han, J., Su, Z., 2020. Structural analysis of strike-slip faults in the Tarim intracratonic basin. *Chinese Journal of Geology* 55, 1–16.
- Yang, P., Liu, K., Liu, J., Yu, S., Wu, L., 2021a. Petroleum Charge History of Deeply Buried Carbonate Reservoirs in the Shuntuoguole Low Uplift, Tarim Basin, West China. *Marine and Petroleum Geology*, 105063.
- Yang, X., Tian, J., Wang, Q., Li, Y., Yang, H., Li, Y., Tang, Y., Yuan, W., Huang, S., 2021b. Geological understanding and favorable exploration fields of ultra-deep formations in Tarim Basin. *China Petroleum Exploration* 26, 17–28.
- Yang, X., Tian, J., Wang, Q., Li, Y., Yang, H., Yong, L., Tang, Y., Yuan, W., Huang, S., 2021c. Geological understanding and favorable exploration fields of ultra-deep formations in Tarim Basin. *China Petroleum Exploration* 26, 12.
- Yassir, N., Addis, M.A., Huffman, A., Bowers, G., 2002. Relationships between Pore Pressure and Stress in Different Tectonic Settings. *Memoirs-American Association of Petroleum Geologists* 76, 79–88.
- Yu, J., Shi, K., Wang, Q., Liu, B., Han, J., Song, Y., Kong, Y., Jiang, W., 2022. Structural diagenesis of deep carbonate rocks controlled by intra-cratonic strike-slip faulting: an example in the Shunbei area of the Tarim Basin, NW China. *Basin Res.* 34, 1601–1631.
- Yun, L., 2021. Controlling effect of NE strike slip fault system on reservoir development and hydrocarbon accumulation and its geological significance in the eastern# br# Shunbei area. Tarim Basin. *China Petroleum Exploration* 26, 41–52.
- Zhang, G., Liu, W., Zhang, L., Yu, B., Wang, L., 2015a. Cambrian-Ordovician prototypic basin, paleogeography and petroleum of Tarim Craton. *Earth Sci. Front.* 22, 269–276.
- Zhang, J., 2011. Pore pressure prediction from well logs: methods, modifications, and new approaches. *Earth Sci. Rev.* 108, 50–63.
- Zhang, J., Zou, H., Li, P., Fu, X., Wang, W., 2015b. A new PVT simulation method for hydrocarbon-containing inclusions and its application to reconstructing paleo-pressure of gas reservoirs. *Petroleum Geology & Experiment* 37, 102–108.
- Zhang, L., Li, C., Luo, X., Zhang, Z., Zeng, Z., Ren, X., Lei, Y., Zhang, M., Xie, J., Cheng, M., 2023. Vertically transferred overpressures along faults in mesozoic reservoirs in the central junggar basin, northwestern China: implications for hydrocarbon accumulation and preservation. *Mar. Petrol. Geol.*, 106152.
- Zhang, Y., Jin, Z., Liu, G., Li, J., 2000. Study on the formation of unconformities and the amount of eroded sedimentation in Tarim basin. *Earth Sci. Front.* 7, 449–457.
- Zhao, J., Li, J., Xu, Z., 2018. Advances in the origin of overpressures in sedimentary basins. *Petroleum Research* 3, 1–24.
- Zheng, H., Hu, Z., Lu, Y., Lin, H., Deng, S., Jia, H., Pu, Y., 2022. Strike-slip faults in marine cratonic basins in China: development characteristics and controls on hydrocarbon accumulation. *Earth Sci. Front.* 29, 224–238.
- Zhou, X., Lü, X., Zhu, G., Cao, Y., Yan, L., Zhang, Z., 2019. Origin and formation of deep and superdeep strata gas from Gucheng-Shunnan block of the Tarim Basin, NW China. *J. Petrol. Sci. Eng.* 177, 361–373.
- Zhu, D., Meng, Q., Jin, Z., Liu, Q., Hu, W., 2015. Formation mechanism of deep Cambrian dolomite reservoirs in the Tarim basin, northwestern China. *Mar. Petrol. Geol.* 59, 232–244.
- Zhu, G., Chen, F., Chen, Z., Zhang, Y., Xing, X., Tao, X., Ma, D., 2016a. Discovery and basic characteristics of high-quality source rocks found in the Yuertusi Formation of the Cambrian in Tarim Basin, China. *Journal of Natural Gas Geoscience* 21–33.
- Zhu, G., Chen, F., Chen, Z., Zhang, Y., Xing, X., Tao, X., Ma, D., 2016b. Discovery and basic characteristics of the high-quality source rocks of the cambrian Yuertusi formation in Tarim Basin. *Nat. Gas Geosci.* 27, 8–21.
- Zhu, G., Hu, J., Chen, Y., Xue, N., Zhao, K., Zhang, Z., Li, T., Chen, Z., 2022. Geochemical characteristics and formation environment of source rock of the lower cambrian Yuertusi formation in well luntan 1 in Tarim Basin. *Acta Geol. Sin.* 96, 1–16.